Tau hyperphosphorylation impairs cooperative binding to microtubules and perturbs organelle trafficking in neurons

Daniel Beaudet[1], Christopher L. Berger[2], and Adam G. Hendricks[1*]

[1]Department of Bioengineering, McGill University, Montreal, Quebec, Canada

[2]Department of Molecular Physiology and Biophysics, University of Vermont, Burlington, Vermont, USA

[*]For correspondence: Adam G. Hendricks adam.hendricks@mcgill.ca

Keywords:

kinesin, dynein, tau, microtubule-associated protein, intracellular transport, hyperphosphorylation, tauopathy, Alzheimer's disease, neurodegeneration, iPSCs, neurons, in vitro reconstitution

Abstract

Tau, a neuronal microtubule-associated protein (MAP), organizes the axonal cytoskeleton and regulates intracellular transport. Tau hyperphosphorylation is closely linked to neurodegeneration in tauopathies including Alzheimer's disease. Tau binds microtubules cooperatively, forming envelopes that restrict access to the microtubule lattice and regulate the activity of motor proteins and other MAPs. However, the effect of disease-related perturbations on tau dynamics and function remains unclear. Using tau phosphomutants in vitro and in live neurons, we show that tau hyperphosphorylation disrupts cooperative binding and dysregulates lysosome transport. Hyperphosphorylated tau does not form envelopes, distributes more uniformly along the axon, and dissociates faster from microtubules. Tau mildly inhibits KIF5C motility, but strongly inhibits KIF1A. Hyperphosphorylation reduces KIF5C inhibition but increases KIF1A inhibition by decreasing processivity and accelerating detachment. Consistent with these effects, hyperphosphorylated tau alters lysosome transport in neurons. While phospho-resistant tau inhibits processive lysosome motility, hyperphosphorylated tau weakens tau-mediated regulation of lysosome transport– mimicking tau knockout neurons that exhibit enhanced processivity. Altogether, hyperphosphorylation disrupts tau envelopes and impairs lysosome trafficking, contributing to defects in degradative pathways that drive neurodegeneration.

Introduction

Tauopathies are a class of neurodegenerative diseases characterized by the misregulation and pathological aggregation of tau, a microtubule-associated protein (MAP) highly expressed in neurons (Binder et al., 1985). Tau regulates the axonal cytoskeleton (Kanai et al., 1992; Chen et al., 1992; Panda et al.,2003; Rosenberg et al., 2008; Chung et al., 2015; Biswas and Kalil, 2018), and acts as a selective barrier on microtubules to direct intracellular transport (Vershinin et al., 2007; Dixit et al., 2008; Vershinin et al., 2008; McVicker et al.,2011; Hoeprich et al., 2014; Hoeprich et al., 2017; Chaudhary et al., 2018; Monroy et al., 2018; Tan et al., 2019; Siahaan et al., 2019; Monroy et al., 2020; Beaudet et al., 2024). Tau's function and microtubule affinity is primarily modulated by alternative splicing (Kellogg et al., 2018; McVicker et al., 2014) and phosphorylation, both of which play key roles in normal development and pathology (Lindwall and Cole, 1984; Mandelkow et al., 1995; Trinczek et al., 1995; Hasegawa et al., 1998; Niewidok et al., 2016; Kanaan and Grabinski, 2021). In Alzheimer's disease and other tauopathies, tau becomes abnormally hyperphosphorylated, reducing its microtubule affinity and promoting aggregation (Schneider et al., 1999; Cho and Johnson, 2003). While tau hyperphosphorylation is a hallmark of disease, its impact on the microtubule cytoskeleton and axonal transport, and in turn neuronal proteostasis, remains unclear.

Tau exhibits both diffusive and cooperative interactions with microtubules. Cooperativity leads to cohesive envelope-like structures (Dixit et al., 2008; Hinrichs et al., 2012; McVicker et al., 2014; Siahaan et al., 2019; Tan et al., 2019; Siahaan et al., 2022). Tau envelopes act as selective, reversible barriers along microtubules, regulating the access of motor proteins and other MAPs to the microtubule. Envelope formation is directed by the intramolecular microtubule lattice spacing between α-β tubulin. Tau does not form envelopes on GMPCPP-polymerized microtubules, which are irreversibly expanded, mimicking the GTP-state, but readily forms envelopes on compacted GDP-lattices or reversibly expanded taxol-lattices (Tan et al., 2019). Most studies investigating tau dynamics have relied on *in vitro* reconstitution assays using purified systems and stabilized microtubules. However, it remains unclear how the nucleotide state distribution and dynamic properties of microtubules in cells influence tau binding. Axonal microtubules are thought to be highly stable, (Black et al., 1984; Brady et al.,1984; Sahenk and Brady, 1987; Lim et al., 1989; Okabe and Hirokawa, 1990; Baas et al., 1991; Ahmad et al., 1993; Li and Black, 1996; Song et al., 2013) but the rate of tubulin turnover and precise nucleotide and lattice compaction landscape of microtubules throughout the axonal cytoskeleton

is not well-characterized. Further, while tau cooperative binding is well-established in purified, in vitro systems, it was an open question if tau forms envelopes in neurons.

The extent of tau's influence on motor proteins depends on several factors including *i)* tau isoform and posttranslational modifications (PTMs), *ii)* the underlying microtubule lattice, and *iii)* the intrinsic properties of the motors themselves. While some motors, such as kinesin-1 and kinesin-3, are strongly inhibited by tau in an isoform- and lattice-dependent manner, others, like kinesin-2 and dynein, can more effectively navigate tau-decorated regions (Dixit et al., 2008; Vershinin et al., 2007; McVicker et al., 2011; Hoeprich et al., 2014; McVicker et al., 2014; Siahaan et al., 2019; Tan et al., 2019; Siahaan et al., 2022). These studies offer important mechanistic insights into how tau regulates individual motor proteins, but it remains unclear how tau's regulatory effects scale when multiple motors work in coordinated ensembles to transport organelles, or whether additional behaviors of tau, like envelope formation, emerge in vivo that alter transport dynamics. Furthermore, the impact of tauopathy-related perturbations on motor protein function are not well understood.

Using in vitro reconstitution and live-cell imaging in iPSC-derived neurons, we find that disease-associated hyperphosphorylation alters tau dynamics on microtubules and impairs intracellular transport. We used phosphomutants in which 14 disease-associated residues were mutated to glutamate (E14) to mimic hyperphosphorylation or alanine (AP) to prevent phosphorylation. Our results show that while WT and AP tau bind microtubules cooperatively, forming envelopes both in vitro and in live neurons, E14 tau interacts more diffusely, has altered axonal localization, and fails to form envelopes. Hyperphosphorylation also affects tau-mediated kinesin regulation. WT and AP tau only mildly inhibit KIF5C motility but increase detachment within envelopes, whereas E14 tau weaken these effects. In contrast, KIF1A is strongly inhibited by either unphosphorylated or phosphorylated tau. Furthermore, in live tau-knockout neurons, lysosomes move more processively than in control neurons. Rescue assays showed that hyperphosphorylation phenocopies tau knockouts, weakening tau-mediated regulation of lysosome transport, resulting in increased processive motility. Combined, our results demonstrate how disease-related hyperphosphorylation weakens the formation of cooperatively-bound tau envelopes on microtubules and perturbs tau-mediated regulation of degradative organelles, which would be expected to cause defects in cargo maturation and protein homeostasis, contributing to neurodegeneration.

Results

Hyper-phosphomimetic tau exhibits diffusive microtubule interactions and reduced tau envelope formation in vitro

We examined how phosphorylation governs tau cooperative binding and envelope formation along microtubules. The phosphostate of tau is strongly dependent on the expression system. Bacterial tau lacks PTMs, while insect and mammalian systems add variable and inconsistent phosphorylation (Siahaan et al., 2024; Fan et al., 2025), making it hard to compare results and understand how disease-related phosphorylation affects tau function. To address this, we used in vitro reconstitution assays with phosphomutants designed to mimic hyperphosphorylation at 14 serine and threonine residues commonly phosphorylated in Alzheimer's disease (Fulga et al., 2007; Steinhilb et al., 2007; Hoover et al., 2010) expressed in mammalian cells. We compared WT tau with hyper-phosphomimetic tau (E14), in which these 14 residues were mutated to glutamate, and phosphorylation-resistant tau (AP), in which they were mutated to non-polar alanine (Fig 1A). This system allowed us to directly assess the impact of disease-associated hyperphosphorylation on tau's microtubule binding without the added complexity and variability introduced by PTMs in other expression systems.

We expressed GFP-tagged tau constructs in COS-7 cells and prepared cell lysates. Lysates were adjusted to ensure an equal tau concentration of 500 nM before they were added to flow chambers containing taxol-stabilized microtubules immobilized on glass coverslips (Fig 1B). Our initial observations, consistent with previous studies, showed that tau binds to microtubules in two distinct kinetic phases: cooperative binding that results in the formation of cohesive envelopes and diffusive binding along the microtubule (Hinrichs et al., 2012; McVicker et al., 2014; Stern et al., 2017; Tan et al., 2019; Siahaan et al., 2022; Cario et al. 2022; Siahaan et al., 2024; Fan et al., 2025). Here, we define tau envelopes as regions along microtubules marked by localized increases in tau intensity that form sharp boundaries with adjacent regions of lower signal. To quantitatively assess the effects of hyperphosphorylation on tau-microtubule interactions, we applied a non-biased approach using Gaussian Mixture Models (GMMs). We performed linescans along microtubules to generate tau-GFP intensity profiles, which we then analyzed using a GMM to identify distinct populations of tau binding. We established a threshold based on the first peak of the GMM distribution plus two standard deviations (Fig 1C), allowing

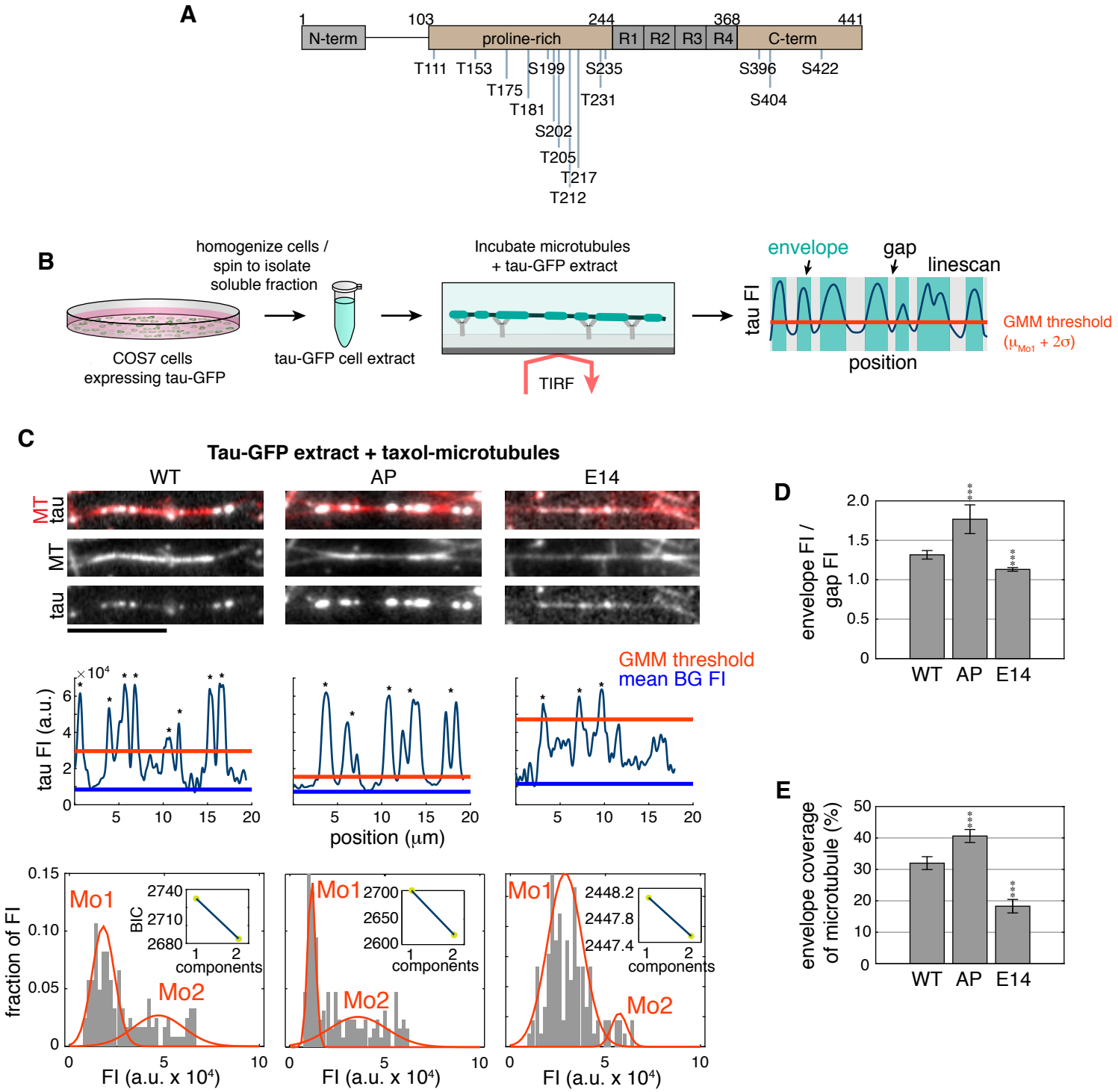
A
1
103
244
368
441
N-term
proline-rich
R1
R2
R3
R4
C-term
T111
T153
T175
T181
S199
S202
T205
T212
T217
S235
T231
S396
S404
S422
B
homogenize cells / spin to isolate soluble fraction
COS7 cells expressing tau-GFP
tau-GFP cell extract
Incubate microtubules + tau-GFP extract
TIRF
envelope
gap
linescan
tau FI
position
GMM threshold
(μ_{Mo1} + 2σ)
C
Tau-GFP extract + taxol-microtubules
WT
AP
E14
MT
tau
GMM threshold
mean BG FI
tau FI (a.u.)
position (μm)
fraction of FI
Mo1
Mo2
BIC
components
FI (a.u. x 10⁴)
D
envelope FI / gap FI
E
envelope coverage of microtubule (%)

Figure 1

Figure 1. Tau hyperphosphorylation results in more diffuse microtubule interactions and reduces tau envelope formation in vitro

A) Structure of 4R0N tau highlighting 14 disease-associated S/T residues mutated to G in pseudo-hyperphosphorylated (E14) tau or to A in phospho-resistant (AP) tau (Hoover et al., 2010). **B)** Schematic illustrating the main steps involved in preparing tau-GFP containing cell extracts and performing reconstitution assays with 500 nM tau (*see* Table 1). Linescans of tau intensity along a microtubule were analyzed using a Gaussian Mixture Model (GMM) to define intensity thresholds distinguishing envelopes from gaps. **C)** Representative images of WT, AP, and E14 tau-GFP on taxol-stabilized microtubules (WT: n=183, AP: n=170, E14: n=170). The indicated n values represent total number of samples over 3–4 replicates. Below the images, corresponding tau intensity plots along microtubules are shown, with horizontal lines indicating the GMM threshold (orange) and mean background fluorescence intensity (blue). Asterisks mark peaks identified as envelopes. Histograms show the distributions of tau fluorescence intensity fitted with a GMM. Insets show Bayesian Information Criterion (BIC) analyses used to determine whether a unimodal or multimodal distribution best describes the data. **D and E)** Plots quantifying the effects of hyperphosphorylation on D) tau envelope intensity and E) percentage of microtubule length covered by envelopes. Error bars indicate 95% CI. Statistical significance was assessed using Student's t-test (*** $p < 0.0001$). Scale bars are 10 μm.

us to differentiate between regions with high tau intensity (envelopes) and regions with lower intensity, indicative of diffusively bound tau (gaps). We found that AP tau formed more robust and frequent envelopes compared to WT tau, whereas E14 significantly reduced both the intensity and frequency of tau envelopes (Fig 1D and E).

To determine whether hyperphosphorylation specifically disrupts tau's cooperative binding or its microtubule binding, we repeated our experiments using GMPCPP-polymerized microtubules. Previous work demonstrated that tau's cooperative binding on taxol-stabilized microtubules is facilitated by its ability to compact the intramolecular spacing between tubulin dimers. Taxol reversibly expands the microtubule lattice, and tau can displace taxol from the microtubule, allowing it to induce lattice compaction. In contrast, GMPCPP-microtubules are irreversibly expanded, preventing tau from inducing lattice compaction and thus cooperative binding (Tan et al., 2019; Siahaan et al., 2022). As expected, tau did not cooperatively bind to GMPCPP-microtubules and form significant envelopes on them, and overall tau intensity was lower than on taxol-stabilized microtubules (Fig S1A–C). E14 tau displayed significantly reduced intensities compared to WT and AP tau, which remained diffusely distributed but at higher intensities (Fig S1C). Together, these results demonstrate that phosphorylation influences not only cooperative binding, but also directly modulates tau's association with microtubules, independent of cooperativity. Phosphorylation likely also regulates tau-induced lattice compaction, in which misregulation of this process could have downstream effects on microtubule stability, as well as interactions with other MAPs and motor proteins.

Tau hyperphosphorylation enhances diffusive microtubule interactions and reduces the formation of envelopes in live neurons

Despite growing evidence for mechanisms that drive tau envelope formation in vitro, it remains unclear whether these structures form in native neuronal environments, what roles they play in regulating the microtubule cytoskeleton and intracellular transport, or how their formation is influenced by tau misregulation. To address these questions, we first sought to determine whether tau forms envelopes in neurons. Given the challenges associated with the expression of multiple tau isoforms in neurons and the variable phosphorylation levels of native tau—both of which have a significant impact on tau-microtubule interactions—we employed a rescue

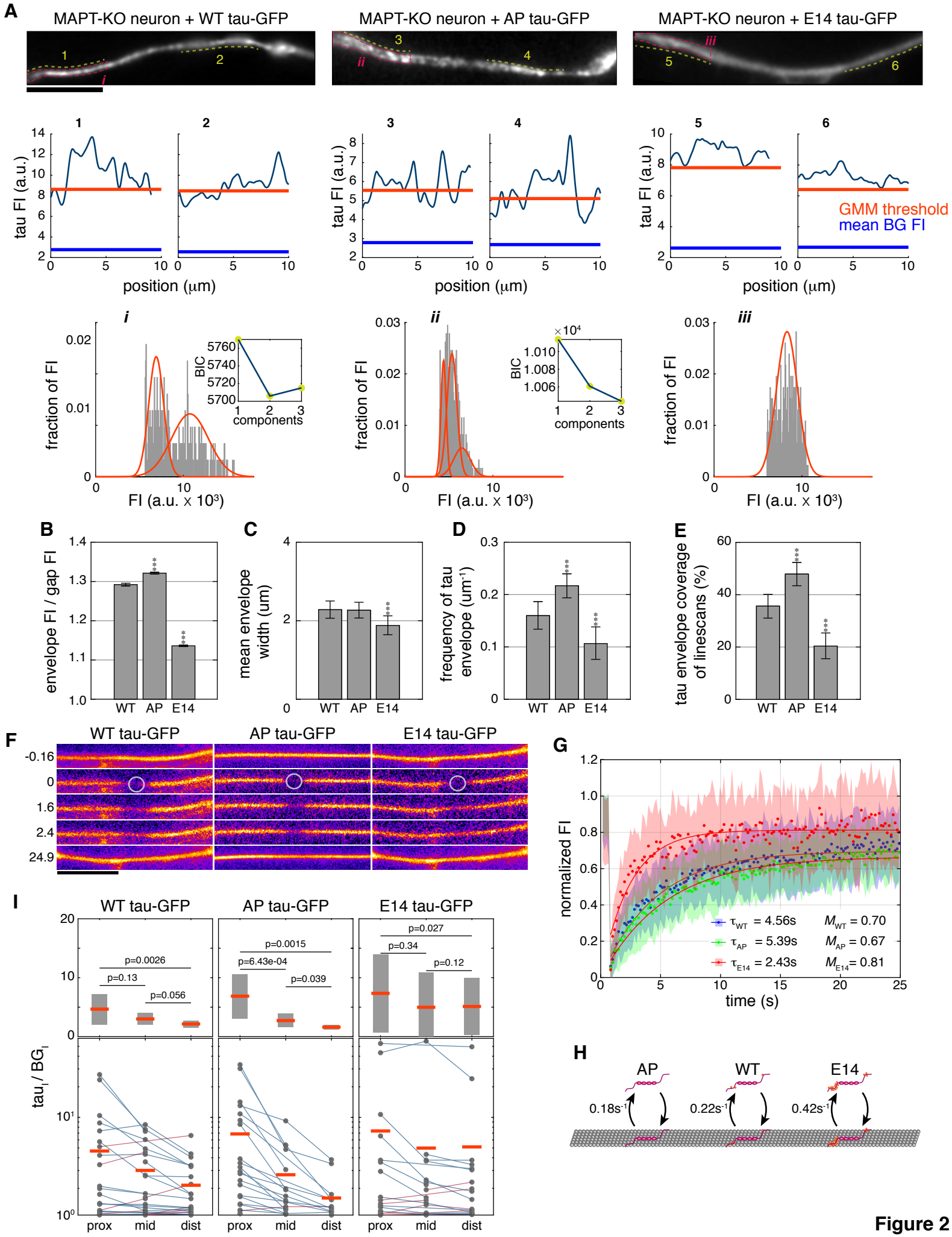
A
MAPT-KO neuron + WT tau-GFP
MAPT-KO neuron + AP tau-GFP
MAPT-KO neuron + E14 tau-GFP
tau FI (a.u.)
position (μm)
GMM threshold
mean BG FI
fraction of FI
FI (a.u. x 10³)
BIC
components
B
envelope FI / gap FI
C
mean envelope width (um)
D
frequency of tau envelope (um⁻¹)
E
tau envelope coverage of linescans (%)
WT
AP
E14
F
WT tau-GFP
AP tau-GFP
E14 tau-GFP
G
normalized FI
time (s)
τWT = 4.56s
τAP = 5.39s
τE14 = 2.43s
MWT = 0.70
MAP = 0.67
ME14 = 0.81
H
AP
WT
E14
0.18s⁻¹
0.22s⁻¹
0.42s⁻¹
I
WT tau-GFP
AP tau-GFP
E14 tau-GFP
p=0.0026
p=0.13
p=0.056
p=0.0015
p=6.43e-04
p=0.039
p=0.027
p=0.34
p=0.12
tauI / BGI
prox
mid
dist

Figure 2

Figure 2. Tau hyperphosphorylation reduces the formation of envelopes in live neurons
A) Representative images of axons with tau envelopes present in iPSC-derived MAPT-KO neurons expressing WT (*n*=39), AP (*n*=39), or E14 (*n*=28) tau-GFP. Each image is a max projection of 10 frames from live timelapse imaging. Images are all oriented so that the soma is towards the left and the distal axon is towards the right. Below, corresponding tau intensity plots from discrete locations (labeled 1–6) are shown. Horizontal lines indicating the GMM threshold (orange) and mean background fluorescence intensity (blue). Histograms of tau fluorescence intensity, fitted with a GMM to define the envelope threshold, are displayed for selected areas (labeled i–iii) marked by magenta ROIs. Insets show BIC analyses for multimodal distributions. **B–C)** Bar plots comparing B) tau envelope intensity and C) the mean envelope width of WT, AP, and E14 tau. **D–E)** Bar plots quantifying tau envelope frequency within D) discrete locations and E) the percentage of total length of axons imaged containing tau envelopes. Error bars indicate 95% CI. **F)** Timelapse images of fluorescence recovery after photobleaching assays of MAPT-KO neurons expressing WT(*n*=20), AP(*n*=21), or E14 (*n*=20) tau-GFP. Circles indicate the bleached regions. Note that tau envelopes are not clearly evident due to shorter exposure times needed for FRAP experiments and due to selection of higher tau-GFP expressing cells to ensure measurable recovery dynamics. **G)** Fluorescence recovery curves of WT (blue), AP (green), and E14 tau (red). Shaded regions indicate SD. The characteristic recovery (τ) and mobile fraction (*M*) are indicated on the plot for each tau construct. **H)** Schematic illustrates how tau phosphorylation influences its dissociation from microtubules. Hyperphosphorylated E14 tau dissociates more readily than WT tau or the phospho-resistant AP tau, which remain more stably bound (Fig S2). **I)** Plots show how the ratio of tau signal in axons of neurons expressing WT (*n*= 37), AP (*n*=32), and E14 (*n*=36) tau over background intensity varies for each tau construct across the proximal, mid, and distal axonal regions. In the bottom plot, blue lines indicate a decrease in the signal from the proximal towards the distal axon, and red lines indicate an increase in tau signal towards the distal axon. The top plot shows the means and grey bars represent SD. Orange bars show means. Wilcoxon signed rank test was used to determine the pairwise comparison of tau intensity between each axonal region as shown and the p-values are indicated in the above inset. The scale bars are 10 μm (A) and 5 μm (F). (*$p < 0.05$, **$p < 0.001$, ***$p < 0.0001$).

approach by overexpressing WT, AP, or E14 tau-GFP in CRISPR-edited tau knockout (MAPT-KO) iPSC-derived neurons at DIV 7–8, when tau is normally expressed within the axon. This strategy allowed us to isolate the effects of hyperphosphorylation on a single tau isoform while avoiding the influence of endogenous tau. Using this approach, we observed the formation of well-defined envelopes in the axon. Tau envelopes are often enriched in discrete segments of several microns in length (Fig. 2A). To quantify the impact of hyperphosphorylation on envelope formation in neurons, we applied the same GMM-based thresholding method used in our *in vitro* studies (Fig. 2A). Quantification showed that WT and AP tau formed envelopes of comparable intensity and width, whereas E14 tau envelopes were less intense and narrower (Fig. 2B, C). Envelope distribution varied across conditions. AP tau exhibited a higher number of envelopes within discrete regions and a greater number of envelope-positive regions along the axon compared to WT tau (Fig. 2D, E). In contrast, E14 tau had the lowest occurrence of envelopes within discrete regions, and envelope-positive regions were infrequently observed throughout the axon (Fig. 2D, E). The observation of envelopes in the native neuronal environment suggests that the axonal microtubule landscape is not uniformly stable, but includes regions where predominantly stable microtubules are interspersed with dynamic or newly formed segments that may serve as regulatory sites for cytoskeletal organization and intracellular transport. Alternatively, differences in underlying post-translational modifications or abundance of other MAPs within these regions may modulate tau's interaction with the microtubule lattice, creating discrete sites where tau envelopes preferentially form.

To further characterize the effects of tau hyperphosphorylation in cells, we performed fluorescence recovery after photobleaching (FRAP) assays to measure tau kinetics on microtubules. Neurons expressing WT, AP, or E14 tau-GFP were photobleached in a diffraction-limited region, and fluorescence recovery was monitored (Fig 2F). AP tau recovered more slowly than WT, while E14 tau recovered the fastest, indicating faster dissociation from microtubules and higher mobility. The 1D geometry of axons constrains diffusion, so we repeated FRAP in COS-7 cells, which have a flatter, more 2D-like geometry. Recovery was ~2× faster in COS-7 cells (Fig S2). Furthermore, in COS-7 cells, WT and AP tau showed clear association and recovery along microtubules, while E14 tau showed no detectable microtubule-bound pool, consistent with our in vitro data showing a lower ratio of E14 tau associated to microtubules than in solution (Fig S1C). These findings suggest that hyperphosphorylation increases tau exchange between the cytosol and microtubules by disrupting cooperative

binding, thereby increasing the dissociation from microtubules and reducing the immobile tau pool (Fig 2H). Thus, phospho-resistant AP tau forms more stable envelopes with lower turnover than WT tau, whereas hyperphosphorylated tau remains highly diffusive and fails to form envelopes.

Tau's affinity for microtubules might also affect its distribution along the axon. In support of this, we found that WT and AP tau is more enriched proximally but E14 tau is more homogenously distributed along the axon (Fig 2I). Although we are rescuing with a single tau isoform, we predict that hyperphosphorylation would likely alter the distribution of native tau in a similar manner. This shift– marked by reduced proximal and increased distal tau– could lead to mislocalization of other tau isoforms, affecting microtubule organization and axonal transport within these regions. For instance, decreased tau in the proximal region might destabilize microtubules, while excessive distal tau could alter microtubule dynamics or lead to impaired distribution of cargoes due to misregulation of transport.

Tau phosphorylation differentially regulates kinesin-1 and kinesin-3 motility along microtubules

Kinesin-1 and kinesin-3 drive the anterograde axonal transport of endosomes, lysosomes, mRNA, and other cargoes (Beaudet et al., 2024; Nagpal et al., 2024). To assess how tau phosphorylation affects intracellular transport, we first examined its impact on individual kinesin motors using TIRF single-molecule motility assays. We analyzed the motility of Halo-tagged KIF5C (kinesin-1) and KIF1A (kinesin-3), expressed in COS-7 cells (Budaitis et al., 2022), on immobilized taxol-stabilized microtubules in the presence of extracts of mock-transfected cells and from cells expressing WT, AP, or E14 tau. The use of mammalian-expressed motors and MAPs provided better protein quality and physiologically relevant PTMs. Results show that KIF5C exhibited increased pausing in the presence of WT, AP, and E14 tau compared to mock extracts without tau (Fig 3A, B). Mean run lengths and velocities were all reduced compared to mock, with AP tau having a slightly stronger reduction on run lengths compared to E14 tau (Fig 3E, S3A and C). However, while tau only slightly reduced KIF5C motility, KIF1A showed significant reductions in both run frequency and processive motility (Fig. 3C, D). Processive runs of KIF1A were rare in the presence of tau. From these rare events, analysis of run lengths

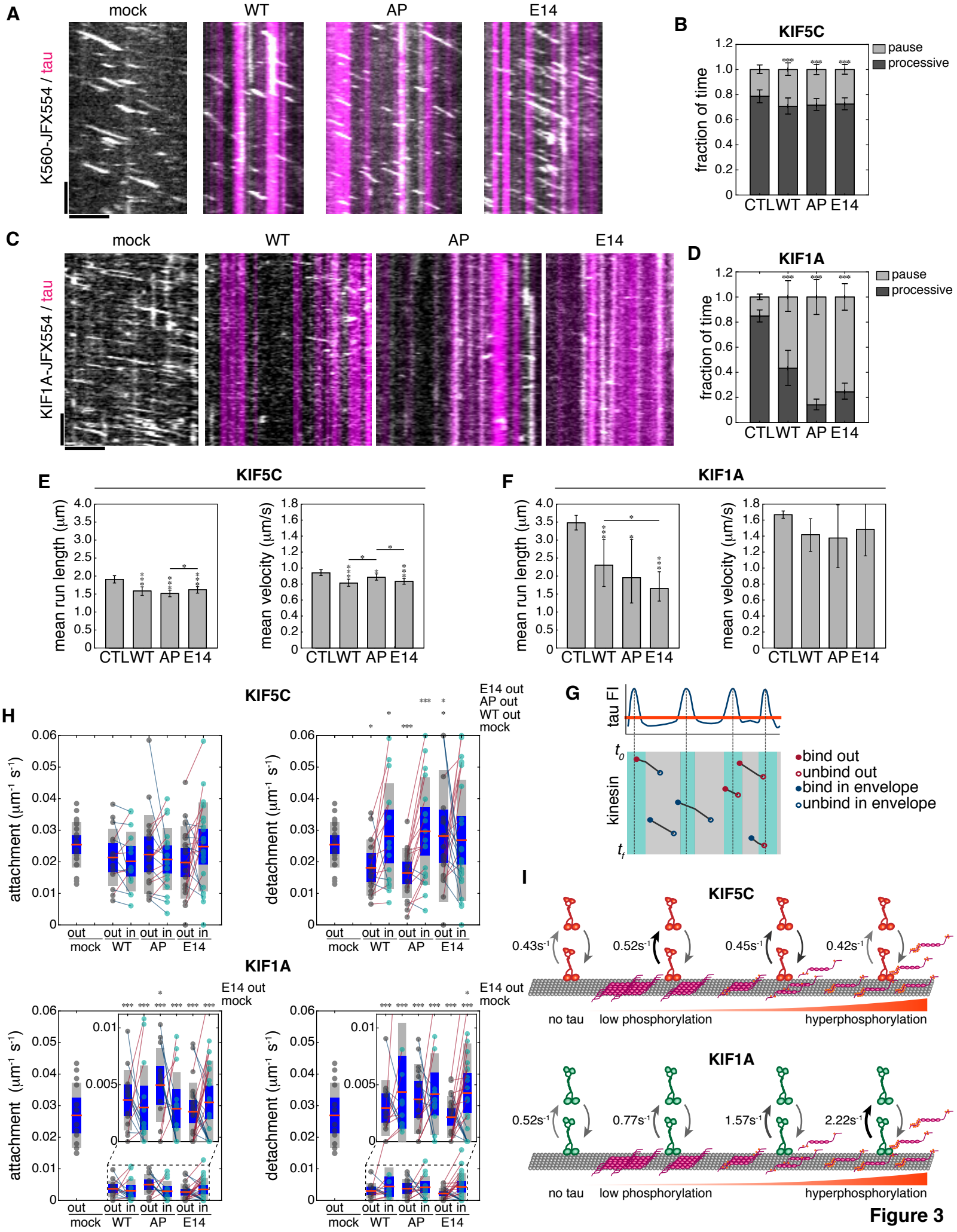
A
mock
WT
AP
E14
K560-JFX554 / tau
B
KIF5C
fraction of time
pause
processive
CTL WT AP E14
C
KIF1A-JFX554 / tau
D
KIF1A
E
KIF5C
mean run length (µm)
mean velocity (µm/s)
F
KIF1A
G
tau FI
kinesin
bind out
unbind out
bind in envelope
unbind in envelope
H
KIF5C
attachment (µm⁻¹ s⁻¹)
detachment (µm⁻¹ s⁻¹)
E14 out
AP out
WT out
mock
out in
KIF1A
I
KIF5C
0.43s⁻¹
0.52s⁻¹
0.45s⁻¹
0.42s⁻¹
no tau
low phosphorylation
hyperphosphorylation
KIF1A
0.52s⁻¹
0.77s⁻¹
1.57s⁻¹
2.22s⁻¹

Figure 3

Figure 3. Tau phosphorylation differentially regulates kinesin-1 and kinesin-3 motility
A and C) Kymographs of constitutively active Janelia Fluor 554 (JFX554)- labelled A) KIF5C(1–560)-JFX554 and C) KIF1A(1–393)-JFX554 motors moving along taxol-stabilized microtubules incubated with mock cell lysate or lysates containing 500 nM WT, AP, or E14 tau-GFP (magenta). KIF5C (mock: n=1016, WT: n=792, AP: n= 1078, E14: n=1203) KIF1A (mock: n= 864, WT: n=173, AP: n=218, E14: n=305) over 3–4 replicates. **B and D)** Bar graphs show the fraction of time that kinesin motors are paused or exhibit processive motility. Error bars indicate 95% CI. **E–F)** Bar graph shows the mean run length and mean velocity of E) KIF5C and F) KIF1A ± WT, AP, E14 tau-GFP. Error bars indicate SEM. **G)** Schematic illustrating the approach used to assess the impact of tau on kinesin-microtubule attachment and detachment. Motors were observed attaching to or detaching from microtubules either within tau envelopes or outside of them. **H)** Paired sample plots show the attachment and detachment frequencies of KIF5C (top) and KIF1A (bottom). Red lines indicate increased frequency inside envelopes compared to outside and blue lines indicate decreased frequencies inside of envelopes. Insets for KIF1A show a zoomed-in view of the attachment and detachment frequencies. Blue bars indicate 95% CI, orange lines mark mean values, and grey bars denote SD. **I)** Schematic illustrating the impact of tau on the detachment kinetics of kinesin motors. KIF5C is weakly inhibited by WT and phospho-resistive tau compared to hyperphosphorylated tau that has a similar dissociation rate compared to KIF5C in mock conditions. Conversely, KIF1A is more strongly inhibited by tau hyperphosphorylation and dissociates at a faster rate compared to WT and AP tau. (*$p < 0.05$, **$p < 0.001$, ***$p < 0.0001$). Horizontal scale bars are 5 μm, vertical scale bars are 5 sec.

showed differences among constructs, with E14 tau being more inhibitory than WT or AP, while mean velocities remained unchanged (Fig. 3F, S3D and F).

We next examined how kinesins behave inside versus outside of tau envelopes by measuring attachment and detachment frequencies. Tau envelopes were identified using the GMM method described above (Fig. 1C), and each kinesin trajectory was classified based on whether it started or ended inside or outside of an envelope (Fig. 3G). KIF5C attached less frequently in the presence of WT and AP tau compared to mock conditions, whereas with E14 tau, attachment frequency was similar to mock conditions (Fig. 3H). Attachment frequency did not significantly differ inside versus outside tau envelopes for any tau construct. However, KIF5C detached more frequently within envelopes containing AP tau compared to WT or E14 tau (Fig. 3H). In contrast, KIF1A showed a ~10-fold reduction in attachment frequency with all tau constructs relative to mock lysate. Attachment was slightly elevated outside of AP tau envelopes compared to E14, while detachment occurred more frequently within E14 tau envelopes than outside (Fig. 3H). Together, these observations suggest that KIF1A is less sensitive to cooperatively bound tau and more sensitive to diffusely bound, non-cooperative tau on microtubules. Dissociation rate constants estimated from KIF5C and KIF1A dwell times also revealed significant differences in the presence of WT, AP, or E14 tau (Fig. S3B and E). While KIF5C dissociated more slowly in the presence of E14 tau compared to WT or AP tau—closely resembling its behavior on tau-free microtubules—KIF1A dissociated more rapidly when exposed to E14 tau (Fig. 3I). These findings support the model that tau acts as a selective barrier to motor proteins, influencing cargo transport based on motor sensitivity. The differential inhibition of kinesin-1 and kinesin-3 suggests tau may gate transport by selectively modulating specific motors. Importantly, tau hyperphosphorylation appears to weaken its inhibitory effect on kinesin-1 while maintaining or enhancing its suppression of kinesin-3, potentially contributing to cargo transport deficits in neurodegenerative disease.

Hyperphosphorylation relieves the inhibition of lysosome motility by tau in neurons

We next examined how tau hyperphosphorylation affects the motility of endogenous cargoes by analyzing lysosome transport in neurons labeled with LysoTracker. We compared lysosome transport across proximal (~50 μm from the soma, avoiding the axon initial segment), mid

(~midpoint), and distal (~50 μm from the axon terminal, avoiding the growth cone) axonal regions in control, MAPT-KO, and MAPT-KO neurons expressing phospho-mutant tau-GFP constructs at DIV 7–8 (Fig. 4A). Kymographs were generated from timelapse images, and lysosome trajectories were analyzed using KymoButler followed by custom MATLAB scripts. In control neurons, ~5% of lysosomes travelled longer than 10 μm with even fewer exceeding 20 μm (Fig 4B, C). Although long-range transport represents only a small fraction of total lysosome movement, it was significantly affected by tau knockout and rescues with the tau phospho-mutants. MAPT-KO neurons exhibited an increased fraction of long-distance retrograde travel, while MAPT-KO neurons expressing either construct showed variable effects. Long distance lysosomes in WT tau-expressing neurons resembled controls, whereas expression of AP tau reduced and E14 tau increased long-range anterograde and retrograde travel (Fig 4C). Although we observed changes in the frequency of long-range lysosome transport, the mean displacement across all trajectories was less affected. E14 tau had the strongest effect in the proximal and distal axon, increasing the mean displacements and cell-to-cell variability relative to WT and AP tau (Fig 4D), suggesting more dynamic and heterogenous motility of lysosomes in neurons expressing E14 tau.

Since this approach relied on transient protein expression, we assessed how the effects on motility varied as a function of tau expression. To classify neurons by expression level, we quantified the ratio of tau-GFP fluorescence in the axon relative to background signal. The effects on lysosome travel distances were dependent on the level of tau expression and scaled differently with each construct. In WT tau-GFP–expressing neurons, lysosomes less frequently traveled long distances at high expression levels (> 5× background signal), compared to those in neurons with lower (1.1–2.0×) or mid-range (2.0 –5.0×) tau expression (Fig S4). In neurons expressing AP tau-GFP, the reduction in lysosome transport distance scaled more steeply with tau expression levels, with long travel distances strongly reduced even at lower expression levels (Fig S4). Conversely, in E14 tau–expressing neurons, long-range lysosome transport was enhanced at low expression levels but reduced at high expression levels, although to a lesser extent than in neurons expressing WT or AP tau (Fig. S4). We also observed that tau knockout neurons with or without expression of tau-GFP had altered lysosome distributions along the axon. In control neurons, lysosomes were most abundant in the proximal axon relative to mid and distal regions (Fig. 4E). In MAPT-KO neurons, lysosomes were as abundant in the mid axon and displayed increased cell-to-cell variance compared to controls (Fig. 4E). WT tau

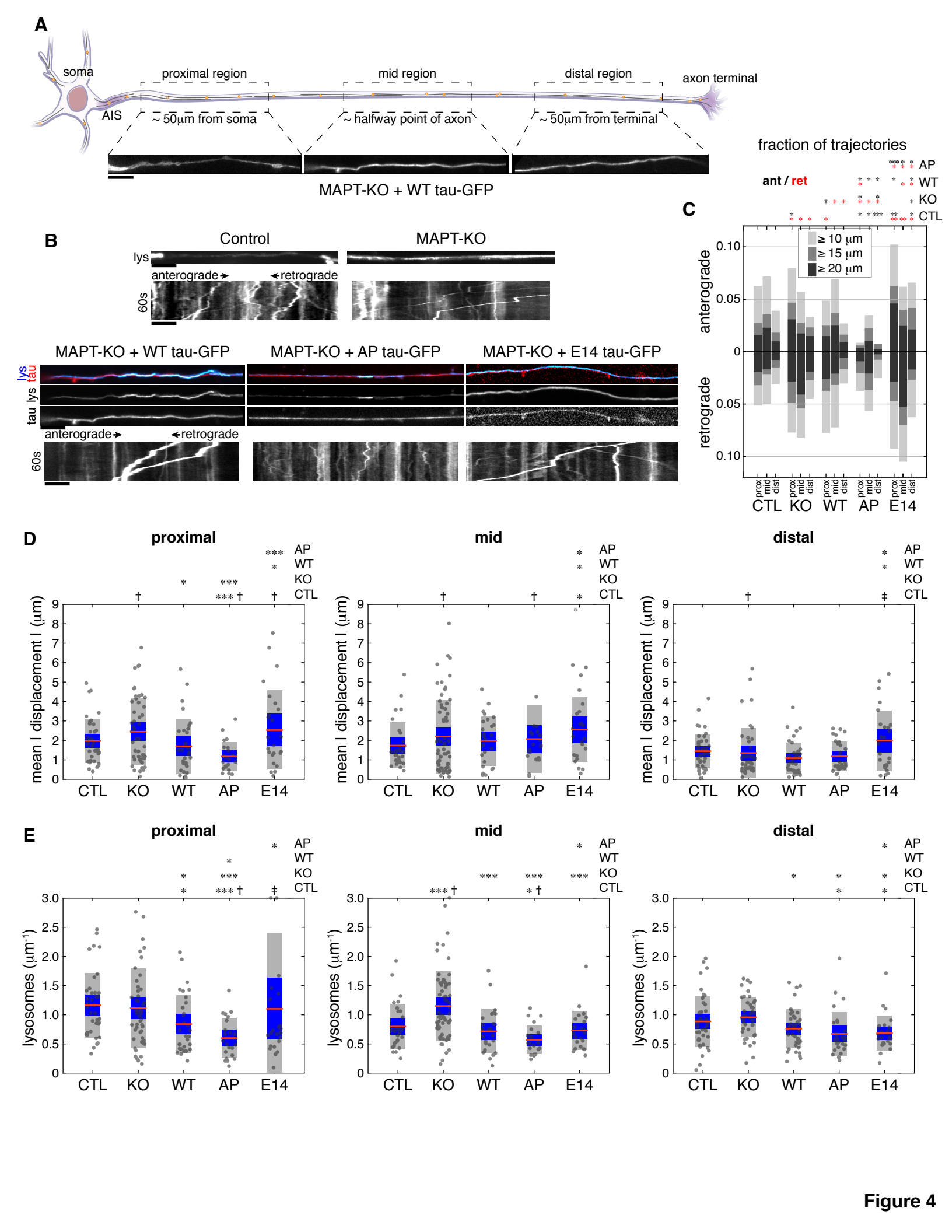
A
soma
AIS
proximal region
mid region
distal region
axon terminal
~ 50µm from soma
~ halfway point of axon
~ 50µm from terminal
MAPT-KO + WT tau-GFP
B
Control
MAPT-KO
lys
anterograde
retrograde
60s
MAPT-KO + WT tau-GFP
MAPT-KO + AP tau-GFP
MAPT-KO + E14 tau-GFP
tau
C
fraction of trajectories
ant / ret
AP
WT
KO
CTL
≥ 10 µm
≥ 15 µm
≥ 20 µm
anterograde
retrograde
prox
mid
dist
CTL
KO
WT
AP
E14
D
proximal
mid
distal
mean l displacement l (µm)
E
lysosomes (µm⁻¹)

Figure 4

Figure 4. Tau perturbations impact the trafficking of lysosomes in neurons
A) Schematic of a neuron indicating the regions where tau's effects on lysosome transport were assessed. Lysosome transport was recorded in proximal, mid, and distal axonal regions. Example images of WT tau-GFP expression are shown from each region. Proximal regions were defined as ~50 μm from the soma, mid-axonal regions as ~halfway along the axon, and distal regions as ~50 μm from the axon terminal. Images are all oriented so that the soma is towards the left and the distal axon is towards the right. The number of cells analyzed under each condition are indicated in Table 2. **B)** Images show mid-axonal tau-GFP signal and max projections of lysosomes (lys) in control, MAPT-KO, and MAPT-KO neurons expressing WT, AP, and E14 tau-GFP. Below kymographs show anterograde and retrograde lysosome transport for each condition. **C)** Bar plot shows the fraction of anterograde and retrograde long-distance trajectories for control (CTL), MAPT-KO (KO), and MAPT-KO neurons expressing WT, AP, or E14 tau-GFP. Above the plot, asterisks represent statistical significance tested for anterograde (black) and retrograde (red) trajectories (* $p < 0.05$, ** $p < 0.001$, *** $p < 0.0001$)**. D and E)** Plots show the D) mean absolute displacements and the E) frequency of lysosomes in the proximal, mid, and distal axon for each condition. Blue bars indicate 95% CI, orange lines mark mean values, and grey bars denote SD. Statistical significance is indicated by asterisks above the at the top of plots (*$p < 0.05$, **$p < 0.001$, ***$p < 0.0001$). Sample variance significance was determined using a two-sample *F*-test for equal variances († $p < 0.05$, $^{\ddagger}p < 0.001$). Scale bars are 10 μm.

expression in MAPT-KO neurons partially restored lysosome distribution, with lysosome abundance comparable in the mid and distal regions, but slightly reduced in the proximal axon relative to controls. AP tau-expressing neurons, however, had significantly fewer lysosomes in the proximal axon and showed reduced variability compared to WT. In contrast, E14 tau-expressing neurons displayed similar lysosome abundance across all axonal regions but increased cell-to-cell variance in the proximal axon (Fig. 4E). These data suggest that lysosomes are normally enriched in the proximal axon and that tau plays a role in promoting lysosome flux toward this region. While some variability may reflect limitations of the rescue strategy, the observed differences in lysosome distribution indicate that tau phosphorylation modulates lysosome biogenesis or cargo maturation within degradative pathways. We propose that phosphorylation fine-tunes tau's influence on cargo transport, enabling precise coordination of lysosome maturation and positioning along the axon. Non-phosphorylated AP tau may restrict lysosome flux, allowing additional time for lysosome maturation before advancing along the axon. Whereas hyperphosphorylated tau may weaken this regulatory control, leading to premature flux and reduced proximal retention. Thus, misregulation of tau could disrupt the function of degradative pathways as a result of mispositioned lysosomes. It is important to note that iPSC-derived neurons at DIV 7–8 have been shown to predominantly express 3R tau isoforms (Iovino et al., 2010; Iovino et al., 2015; Sposito et al., 2015). In our rescue experiments, however, we introduce 4R0N tau. Although we observed minimal differences in displacements and lysosome abundance between MAPT-KO neurons expressing WT (4R) tau and control neurons (3R), there is still the possibility that isoform differences influence the severity of transport phenotypes, particularly under conditions of increased phosphorylation.

Lysosomes alternate between periods of stationary, diffusive, and processive movement. Trajectories were segmented by identifying directional reversal events and the intervening periods were characterized as stationary (less than 0.16 μm, within the tracking uncertainty), diffusive (between 0.16 μm and 1.2 μm), and processive (greater than 1.2 μm) (Fig 5A). In control neurons, lysosomes were primarily in diffusive or stationary states, with a small fraction of time exhibiting processive movement, a trend consistent across all regions (Fig 5A, B). MAPT-KO neurons exhibited a progressive increase in stationary lysosome behavior and a corresponding decrease in processive movement toward the distal axon. In neurons expressing AP tau, lysosomes exhibited increased diffusive behavior and in certain cases were less

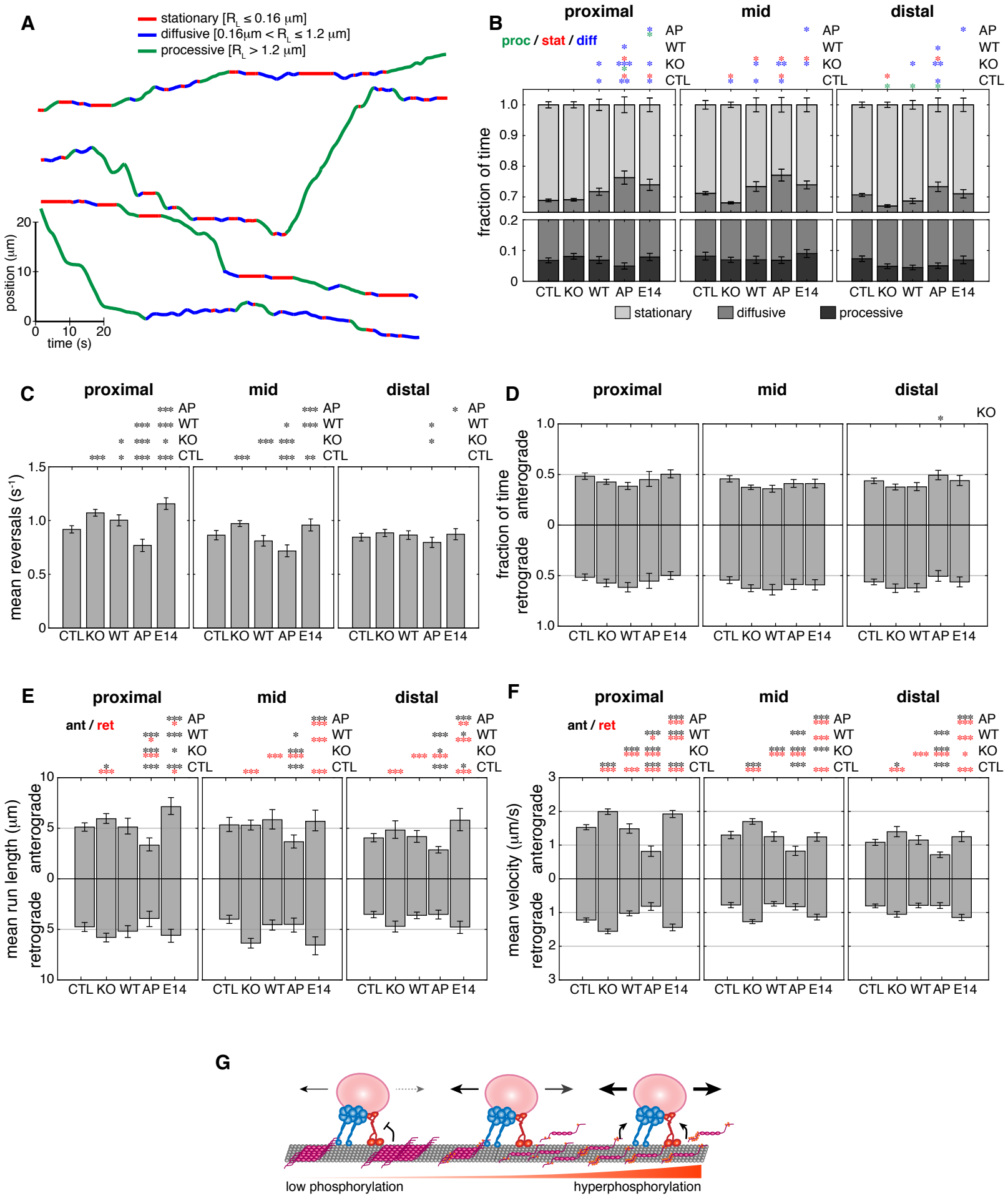
A
stationary [R_L ≤ 0.16 μm]
diffusive [0.16μm < R_L ≤ 1.2 μm]
processive [R_L > 1.2 μm]
position (μm)
time (s)
B
proximal
mid
distal
proc / stat / diff
AP
WT
KO
CTL
fraction of time
CTL KO WT AP E14
stationary
diffusive
processive
C
mean reversals (s⁻¹)
D
fraction of time
anterograde
retrograde
E
ant / ret
mean run length (μm)
F
mean velocity (μm/s)
G
low phosphorylation
hyperphosphorylation

Figure 5

Figure 5. Tau hyperphosphorylation relieves inhibition of processive lysosome motility in neurons

A) Shown are examples of lysosome trajectories segmented into stationary (red), diffusive (blue), and processive (green) motility based on run length. Stationary segments were defined as periods between two reversal events with a run length (R_L) < 0.16 μm; diffusive segments as those with run lengths between 0.16 μm and 1.2 μm; and processive segments as those > 1.2 μm. **B)** Plots show the fraction of time spent in each transport mode for control (CTL), MAPT-KO (KO), and MAPT-KO neurons expressing WT, AP, and E14 tau-GFP in the proximal, mid, and distal axon. Error bars represent 95% CI. Statistical significance is indicated above the plots for comparison of the fraction of processive (proc; green) diffusive (diff; blue), and stationary (stat; red) time for each condition. **C–D)** Bar plots show C) the mean reversal frequency of lysosomes, D) and the fraction of time of anterograde or retrograde directed processive motility. **E–F)** Bar plots show E) the mean run lengths and F) mean velocities of processive runs of lysosomes for each condition in proximal, mid, and distal axonal regions. Error bars in C), E), and F) indicate SEM and in D) indicate 95% CI. The number of trajectories and cells analyzed under each condition are indicated in Table 2. **G)** Schematic summarizing the impact of tau hyperphosphorylation on bidirectional lysosome transport in neurons. Low levels of tau phosphorylation reduce processive anterograde transport throughout the axon but has a weaker impact on retrograde transport, whereas hyperphosphorylated tau enhances lysosome motility in both directions across the axon, similar to the effects observed in tau knockout conditions. Statistical significance is shown above each plot, where red asterisks indicate comparisons of retrograde transport and black asterisks indicate comparisons of anterograde transport. (* $p < 0.05$, ** $p < 0.001$, *** $p < 0.0001$).

processive (Fig 5B). Although these data did not reach statistical significance, when averaged across trajectories and cells, the data suggest a trend of stronger effects in the proximal axon, with E14 tau increasing processive time, AP tau reducing it, and WT tau exhibiting an intermediate effect. Lysosomes are bidirectional cargoes that frequently undergo directional reversals. MAPT-KO neurons exhibited an increased frequency of directional reversals in the proximal and mid axon compared to control neurons (Fig 5C). AP tau significantly reduced the reversal frequency, while E14 tau enhanced reversals, with the most significant effects observed in the proximal and mid axon (Fig 5C). These data suggest that non-phosphorylated AP tau promotes more diffusive or stationary transport modes, whereas E14 tau may restore aspects of processivity but impairs directional persistence. An important consideration is that while these measurements capture a snapshot of lysosome dynamics, the cumulative effects of altered transport and distribution over longer timescales are likely to be more pronounced.

The effects of tau on individual kinesin and dynein motors have been well characterized in single-molecule motility assays, but it is less clear how tau effects endogenous cargoes such as lysosomes or other endocytic vesicles that are transported by multiple motor types and variable motor copy numbers (Jordens et al., 2001; Brown et al., 2005; Loubéry et al., 2008; Rosa-Ferreira and Munro, 2011; Bentley et al., 2015; Pu et al., 2016; Beaudet et al., 2024). To better understand how tau hyperphosphorylation affects the coordinated activity of motor teams driving bidirectional transport, we analyzed the processive segments of lysosome motility. In most neurons analyzed, lysosomes showed a slight retrograde bias (Fig 5D). Although lysosomes in MAPT-KO neurons spent less time in the processive state overall, processive runs exhibited comparable anterograde run lengths but significantly longer retrograde run lengths (Fig 5E). Additionally, mean velocities in both anterograde and retrograde directions were increased compared to control neurons (Fig 5F). In neurons expressing WT tau, processive lysosome motility closely resembled that of control neurons, with comparable run lengths and velocities in both directions across most axonal regions (Fig. 5E, F).

AP and E14 tau had distinct effects on processive motility. AP tau generally suppressed anterograde processive transport while having weak or no effect on retrograde transport (Fig. 5E, F). Conversely, E14 tau either rescued WT-like transport characteristics or in most regions enhanced lysosome run lengths and velocities.

These findings support a model in which non-phosphorylated tau suppresses motor-driven transport, whereas hyperphosphorylated tau alleviates this inhibition and functionally mimics tau deletion (Fig. 5G). Due to its proximal enrichment and tighter microtubule binding along the axon (Fig. 2H, I), AP tau strongly inhibits both anterograde and retrograde transport in the proximal region, with reduced inhibition of retrograde movement in the mid and distal axon. In contrast, E14 tau, which binds microtubules more weakly and distributes more uniformly along the axon (Fig. 2H, I), relieves inhibition and, in many cases, enhances both anterograde and retrograde motility across axonal compartments. Collectively, these data support a model in which tau phosphorylation alters microtubule affinity, leading to changes in the axonal accumulation and regional concentrations of tau. These alterations modulate tau's capacity to act as a roadblock and influence its effect on specific motor proteins driving axonal transport.

Discussion

Tau hyperphosphorylation is a hallmark of Alzheimer's Disease and associated with the aggregation of tau into neurofibrillary tangles. Here, we focused on the functional consequences of tau hyperphosphorylation on microtubules—either as a cytoskeletal organizer or as a regulator of intracellular transport— prior to aggregation. We find that hyperphosphorylation disrupts tau's ability to form envelopes on microtubules and alters microtubule-based transport. Tau binds cooperatively in live neurons, consistent with its behaviour on stabilized microtubules in vitro (Figs. 1 and 2). Disease-related hyperphosphorylation ablates cooperative binding and enhances tau's dissociation from microtubules (Figs. 1 and 2). Tau hyperphosphorylation also has different effects on different kinesin motors. KIF5C motility is mildly inhibited by mammalian expressed tau compared to KIF1A that is strongly inhibited (Fig. 3). Hyperphosphorylation reduces KIF5C dissociation from microtubules, while it increases that of KIF1A (Fig. 3), suggesting that misregulation of tau could alter axonal trafficking by disrupting kinesin activity. In agreement, we found that hyperphosphorylation weakens tau-mediated inhibition of lysosome transport in neurons. While unphosphorylated tau acts as a strong barrier to anterograde lysosome movement, hyperphosphorylated tau alleviates this inhibition, mimicking tau knockout conditions in which lysosomes moved more processively (Figs. 4 and 5). These disruptions in transport likely lead to impairments of degradative pathways and protein homeostasis, which contribute to neuronal dysfunction and degeneration in tauopathies.

Isolating the effects of tau phosphorylation presents significant challenges. Tau is phosphorylated at numerous residues and at different developmental stages, and individual tau molecules often exhibit heterogeneous phosphorylation patterns (Lindwall and Cole, 1984; Mandelkow et al., 1995; Trinczek et al., 1995; Hasegawa et al., 1998; Siahaan et al., 2024; Fan et al., 2025). There are six tau isoforms expressed in the mature human brain (Weingarten et al., 1975; Goedert et al., 1988; Goedert et al., 1989a; Goedert et al., 1989b; Andreadis et al., 1992), further complicating efforts to dissect specific aspects of its function and regulation. To isolate effects of tau phosphorylation, we employed phospho-mimetic and phospho-resistive mutants of tau (Hoover et al., 2010). To avoid effects from various endogenous tau isoforms, we used either COS-7 cells to express tau-GFP for *in vitro* studies, since tau is not endogenously expressed in these cells, or expressed the phosphomutant tau proteins in MAPT-KO neurons to assess transport phenotypes. These systems enabled us to examine tau function in a near-physiological environment—preserving relevant cytosolic factors and PTMs—while isolating the

effects of hyperphosphorylation of a single tau isoform from those of endogenous tau. While this study focused on one isoform, other tau isoforms differ in microtubule affinity and likely undergo distinct phosphorylation patterns. Typically, iPSC-derived neurons at DIV 7–8 predominantly express 3R tau, with 4R tau appearing later (Iovino et al., 2010; Iovino et al., 2015; Sposito et al., 2015). Since 3R tau has a lower affinity for microtubules but more strongly inhibits kinesin and dynein motors compared to 4R tau (Vershinin et al., 2008; McVicker et al., 2011; McVicker et al., 2014), hyperphosphorylation may have more severe effects in mature neurons where 3R and 4R tau are equally expressed. Future work is needed to explore how these isoforms interact, influence each other's microtubule binding and cooperative assembly, and how phosphorylation heterogeneity among tau molecules (Siahaan et al., 2024; Fan et al.,2025) contributes to disease progression in tauopathies.

Our findings contribute to the growing body of evidence that the N-terminal projection domain of tau modulates cooperative binding to microtubules (Tan et al., 2019; Siahaan et al., 2019; Siahaan et al., 2022), and that mutations or modifications in this region impair tau's ability to form envelopes (Cario et al., 2022; Siahaan et al., 2024) and function as an effective regulator of intracellular transport (Kanaan et al., 2012; Stern et al., 2017; Balabanian et al., 2022). Previous studies show that tau binds to compacted GDP-lattices or cooperatively binds and compacts taxol-stabilized microtubule lattices, but cannot bind cooperatively to GMPCPP-microtubules (Tan et al., 2019). Consistent with this, we observed robust envelope formation on taxol-microtubules but not on GMPCPP-microtubules (Figs. 1 and S1), indicating that lattice compaction is required for cooperative binding. The projection domain likely facilitates this process either by modulating the microtubule-binding repeats or by promoting tau–tau interactions that drive cooperative binding. Supporting the latter model, the pathogenic R5L mutation was shown to disrupt cooperative binding by altering the structure of the projection domain without affecting the microtubule-binding repeats (Cario et al., 2022), implicating the projection domain as a key mediator of tau–tau interactions. Consistent with this, our data show that cooperative binding via the projection domain is essential for maximizing tau association with microtubules (Fig. 1). Similarly, we found that phosphorylation at sites primarily within the projection domain significantly reduced cooperative binding, diminished envelope formation, and increased tau dissociation from microtubules, indicating weakened binding affinity (Fig. 2F–G, Fig. S2).

If phosphorylation within this region strictly regulates cooperative binding, we would expect no effect of hyperphosphorylation on tau binding to GMPCPP-microtubules, where cooperative binding is absent. However, this is not the case, since we found that hyperphosphorylated tau exhibited significantly reduced binding to GMPCPP-microtubules compared to WT and phospho-resistant tau (Fig. 1G–I). This suggests several possibilities: (1) the projection domain may allosterically regulate the microtubule-binding repeats to control direct microtubule interactions, (2) phosphorylation within the projection domain and C-terminus may reduce the intrinsic affinity of tau for the microtubule lattice, or (3) phosphorylation may impair tau's ability to compact the underlying lattice, thereby preventing envelope formation. Taken together, our findings reconcile multiple lines of evidence to establish the projection domain as a critical regulator of both tau–tau and tau–microtubule interactions. Phosphorylation at sites within this region modulate these interactions and controls tau's binding dynamics. Disruption of this regulatory mechanism increases the volatility of tau–microtubule interactions, potentially contributing to microtubule destabilization and impaired intracellular transport.

Our data demonstrate that tau hyperphosphorylation is associated with impaired axonal transport. Previous single-molecule studies established that tau inhibits kinesin-1 and kinesin-3 motility, while having less of an effect on kinesin-2 and dynein. Based on these findings, conditions that reduce tau's microtubule association, such as hyperphosphorylation or tau knockout, would be expected to enhance anterograde transport of cargoes driven by kinesin-1 and kinesin-3 motors. Conversely, dephosphorylation, which strengthens tau's association with microtubules, would be expected to further inhibit anterograde transport. Consistent with this model, our results show that both tau knockout and tau hyperphosphorylation result in increased anterograde and retrograde motility. Whereas phospho-resistant tau reduced anterograde transport and had little-to-no impact on retrograde transport. These findings suggest that hyperphosphorylated tau fails to perform its normal function as a regulatory barrier on microtubules. The observed increase in retrograde transport may indicate that tau also modulates dynein activity, and that hyperphosphorylation either relieves tau-mediated inhibition of dynein or indirectly alters kinesin function in a way that favors retrograde transport. One explanation is that cargoes are transported by teams of multiple motors, including force-producing motors and those that act as tethers (Feng et al.,2018; Arpag et al.,2019). For instance, increased inhibition of kinesin-3 by hyperphosphorylated tau could reduce its tethering capacity, shifting the balance in favor of dynein-driven retrograde transport. This is consistent

with the increased retrograde lysosome motility we observed in E14 tau-expressing neurons. Alternatively, mislocalization of tau along the axon may permit increased binding of other MAPs, such as MAP7. MAP7 competes with tau for microtubule lattice binding and has been shown to enhance kinesin-1 motility while inhibiting kinesin-3 (Monroy et al., 2018). These opposing effects may contribute to enhanced anterograde transport by promoting kinesin-1 processivity or increased retrograde transport by limiting kinesin-3 activity, while having a comparatively minor impact on dynein-mediated transport. This suggests that cargo-specific motor compositions and their differential sensitivities to tau (Beaudet et al., 2024) may underlie the observed changes in transport dynamics when tau is hyperphosphorylated.

Taken together, our findings show that tauopathy-related hyperphosphorylation weakens tau's interaction with microtubules, reducing its ability to form cohesive envelopes and regulate axonal transport. Beyond impaired lysosome trafficking, this disruption likely affects signaling and other maintenance pathways essential for axonal health and function. Our results suggest a potential pathway, where prior to oligomerization and late-stage aggregation, hyperphosphorylated tau first impairs transport, which then contributes to axonal decline. As aggregation progresses, these effects are amplified, leading to further trafficking defects, axonal blockages, inflammation, and ultimately neurodegeneration. While our study highlights early phenotypes of tauopathy, how these changes interact with other disease mechanisms remains unclear. Future work should define how tau misregulation reshapes the neuronal environment and cooperates with additional pathological processes to drive neurodegeneration. Overall, our results suggest that the disruption of axonal transport—caused by tau's impaired association with microtubules—is one of the earliest drivers of neurodegeneration.

Methods

DNA constructs

The pRK5-EGFP-Tau (Addgene plasmid # 46904), pRK5-EGFP-Tau AP (Addgene plasmid # 46905), and pRK5-EGFP-Tau E14 (Addgene plasmid # 46904) plasmids were gifts from Karen Ashe. KIF1A(1-393)-LZ-HALO reported in (Budaitis et al., 2021) was generously provided by Kristen Verhey (U. Michigan). KIF5C(1-560)-HALO reported in (Twelvetrees et al., 2016) was generously provided by Erika Holzbaur (U. Pennsylvania).

Cell culture and transfection

COS-7 monkey kidney fibroblast cells (ATCC) were maintained in DMEM (Gibco), supplemented with 10% fetal bovine serum (Thermo Fisher Scientific) and 1% GlutaMAX (Gibco) and cultured in MatTek glass-bottom dishes (No. 1.5 Coverslip) (MatTek Corporation, Ashland, MA) at 37°C with 5% CO_2 for 24–48 h before transfection. Cells were then transfected with 500 ng of DNA plasmid prepared in OPTI-MEM Reduced Serum (Life Technologies), using Lipofectamine LTX with Plus-Reagent, according to the manufacturer's instructions (Invitrogen, Thermo Fisher Scientific) for 24 h prior to imaging or homogenization.

Human neurons were induced from iPSC control and MAPT-KO AIW002-02 lines. The iPSCs were obtained from the C-BIG repository (Montreal Neurological Institute-Hospital, Montreal, QC, Canada) and were generated from the PBMC of a control 37-year-old male donor. MAPT knockout was achieved by CRISPR-Cas9 and verified by PCR and sequencing. Guide RNAs (gRNAs) were designed using "optimized CRISPR design" tool (www.crisp.mit.edu). The locations of gRNA1(GGATAAGTTCTGAGGAGTGT) and gRNA2 (TGATCTGGGCCTGCTGTGCA) were around exon 2 with ATG start codon. Oligonucleotides with Bsb1 cleavage overhang were ordered from Life Technologies, annealed and cloned into the PX459 Cas9/puromycin vector (Addgene plasmid #48139). iPSCs were characterized to ensure correct genotyping, pluripotency, and screened for microbiology/virus. iPSCs were maintained in mTeSR Plus media (STEMCELL Technologies, Vancouver, BC) on Matrigel (Corning, Corning, NY) coated culture dishes using Gentle Cell Dissociation Reagent (STEMCELL Technologies) for passaging. The iPSCs were cultured for ~ 30 days in STEMdiff SMADi medium (STEMCELL Technologies) to induce the formation of neuronal progenitor cells

(NPCs). NPCs were dissociated from culture dishes (Accutase Cell Dissociation Reagent) and seeded on poly-l-ornithine (PO) (10 μg/ml)/laminin (15 μg/ml)-coated MatTek glass-bottom dishes (No. 1.5 Coverslip) at 37°C with 5% CO_2 in BrainPhys differentiation media (STEMCELL Technologies) at about 2,000 cells per cm^2. Six days after seeding, the cells were transfected with lipofectamine LTX reagent at a 3:1 reagent:DNA according to the manufacturer's instructions then imaged at 7–8 days following terminal differentiation induction.

Live cell imaging

To capture lysosome dynamics, neurons were treated with 70 nM LysoTracker (Thermo Fisher Scientific, Waltham, MA) for 30 minutes at 37°C with 5% CO_2 prior to replacing the media with BrainPhys containing 15 mM HEPES (H3375, Millipore Sigma). Live cell imaging was performed on an Eclipse Ti-E inverted microscope (Nikon) with custom optics for total internal reflection fluorescence (TIRF) and imaged using EMCCD camera (iXon U897; Andor Technology) maintained at 37°C. Time lapse recordings were acquired with 120 msec exposures using a 640 nm laser (100 mW) set at 1% power for 120 sec per cell using NIS-Elements acquisition software (Nikon). To image tau-GFP envelopes in neurons, imaging was performed as described but acquired with 500 msec exposures for 30 seconds using a 480nm laser set at 2% laser power. To measure tau-GFP expression in neurons a single frame was taken with 500nm exposure using a 480nm laser set at 2% laser power. Image files were exported as TIFFs, which were opened with ImageJ (NIH) and lysosomes were tracked by kymograph analysis. Briefly, linescans were traced over the axon to generate kymographs, which were then analyzed using KymoButler (Jakobs et al., 2019) to identify individual lysosome trajectories. The coordinates of each trajectory were then imported into MATLAB (The MathWorks) to analyze the mode of transport, directionality, displacement, and number of reversals for all trajectories within cells using custom scripts.

FRAP

COS-7 cells or neurons at 7–8 DIV expressing WT, AP, or E14 tau-GFP were used to assess tau kinetics in live cells. FRAP experiments were performed at 37 °C using a DeltaVision OMX system equipped with a 100×/1.40 NA objective lens and an EMCCD camera (Evolve, Photometrics). Prior to photobleaching, 5 pre-bleach images were acquired with 100 ms

exposure. Photobleaching was performed within a diffraction limited spot using 50% 488 nm laser power for 50 ms. Fluorescence recovery was then recorded for 100 frames for COS-7 cells or 150 frames for neurons using 31% 488 nm laser power and 100 ms exposure per frame. Fluorescence recovery curves were generated using ImageJ, and background-corrected to account for acquisition-related photobleaching. Fluorescence recovery data were fit to a single-exponential function described by equation (1):

$$F(t) = M(1 - e^{\frac{-t}{\tau}}) \quad (1)$$

where $F(t)$ is the fluorescence intensity at time t, M is the mobile fraction, τ is the characteristic recovery time and the dissociation rate constant (k_{off}) is described by equation (1.1):

$$k_{off} = -\frac{1}{\tau} \quad (1.1)$$

COS-7 cell extract preparation

To prepare tau-GFP–containing cell extracts, COS-7 cells expressing WT, AP, or E14 tau-GFP were harvested 24 h post-transfection. For extracts containing kinesin motor proteins, COS-7 cells expressing Halo-tagged KIF5C or KIF1A were labeled with Janelia Fluor JFX554 ligand (Promega) using the manufacturer's rapid labeling protocol and collected 24 h post-transfection. Cells were incubated with 200 nM JFX554 for 30 min, rinsed 2× with pre-warmed DMEM, followed by 2× PBS to remove residual media. Cells were then collected using a cell scraper in ice-cold lysis buffer (10 mM PIPES, 50 mM potassium acetate, 4 mM $MgCl_2$, 1 mM EGTA, pH 7.0), supplemented with protease inhibitor cocktail (BioShop), 10 mM DTT, and 0.5% Triton X-100. For motor-containing extracts, 1 mM MgATP was also included. Cell suspensions were incubated on ice for 1 min, then centrifuged at 1,000 × g for 10 min at 4 °C. Supernatants were transferred to fresh ice-cold microcentrifuge tubes and spun at 16,000 × g for 10 min at 4 °C. The concentration of tau-GFP in the extracts was determined by measuring absorbance at 488 nm using a Nanodrop spectrophotometer, applying an extinction coefficient of 56,000 $M^{-1}cm^{-1}$ (Table 1). The resulting soluble fractions containing tau-GFP or fluorescently labeled kinesin motors were aliquoted, flash-frozen in liquid nitrogen, and stored at –80 °C for subsequent experiments.

Microtubule polymerization

To prepare taxol-stabilized microtubules, polymerization reaction mixtures containing 8% Alexa647-labeled tubulin and 92% unlabeled tubulin (final concentration of 5 mg/mL) in BRB80 (80 mM K-Pipes, 1 mM $MgCl_2$, 1 mM EGTA, pH 6.8) supplemented with 1 mM GTP were prepared on ice thenn incubated for 25 mins at 37°C. Microtubules were then stabilized with 20 µM Taxol (Cytoskeleton) and incubated for 25 mins at 37°C. For GMPCPP-microtubules, reaction mixtures were mixed with 1mM GMPCPP (Jena Bioscience, Jena, Germany) for 60 minutes. Microtubules were cleared 2X by pelleting them at 10,600*g* for 5 mins at RT then washed with T-BRB80 (BRB80 supplemented with 20 µM Taxol).

In vitro reconstitution assays

Flow chambers were first incubated with anti-β-tubulin (T4026 clone TUB2.1, Sigma) diluted 1:25 in BRB80 for 5 mins. Chambers were then treated with F-127 for 5 mins and washed 2X with T-BRB80. Fluorescently-labeled microtubules were added to the chambers and incubated for 5 mins at RT. Unbound microtubules were washed out with 2X T-BRB80. Tau-GFP containing cell extracts were diluted 2-fold in MAB supplemented with 0.2 mg/ml BSA, 10 mM DTT, 20 mM Taxol, 15 mg/ml glucose, ≥ 2000 units/g glucose oxidase, ≥ 6 units/g catalase, and 1 mg/ml casein and flown through the chamber containing microtubules and imaged in TIRF. To image tau-GFP envelopes in vitro, images were acquired with 500 msec exposures for 30 seconds using a 480nm laser set at 2% laser power. Envelope analysis was performed using images of sum projections of stacks consisting of 10 frames with custom MATLAB scripts.

To capture kinesin motility dynamics, motility reaction mixtures containing 3 ul of KIF5C-JFX or KIF1A-JFX motor-containing cell extracts were mixed with tau-GFP cell extracts diluted 2-fold in MAB supplemented with 0.2 mg/ml BSA, 10 mM DTT, 20 mM Taxol, 15 mg/ml glucose, ≥ 2000 units/g glucose oxidase, ≥ 6 units/g catalase, 1 mg/ml casein, and 5mM MgATP and flown through the chamber containing microtubules and imaged in TIRF. To image kinesin motility, images were acquired for 2 minutes with 120 msec exposure using 640 nm laser set at 10–15% laser power. Image files were exported as TIFFs, linescans were traced over microtubule images to generate kymographs of kinesin motility, which were then analyzed using KymoButler and custom MATLAB scripts.

Envelope analysis

To analyze tau envelopes, linescans were traced along microtubules incubated with WT, AP, or E14 tau-GFP, and fluorescence intensity profiles were generated. Tau intensity distributions were then fit using a Gaussian mixture model (GMM) to determine the intensity threshold for defining envelopes. The optimal number of components in each distribution was selected based on the Bayesian Information Criterion (BIC). Microtubules with tau envelopes were identified by multi-component fits, whereas those lacking envelopes were best fit by a single-component model (Fig. 1C). The envelope detection threshold was defined as the intensity corresponding to the first GMM mode plus two standard deviations (σ). Intensities above this threshold were classified as envelopes, while those below were considered diffuse tau between envelopes. A similar analysis was performed to identify and quantify tau envelopes in neurons, with the exception that 10 µm linescans were drawn in envelope-positive regions, which were manually selected based on the degree of fluorescence intensity variation along the axon.

Analysis of kinesin kinetics on tau-microtubules

To quantify the attachment and detachment frequencies of kinesins on tau-decorated microtubules, tau envelopes were first identified as described above. Kymograph analysis was then used to determine the start and stop positions of each kinesin trajectory, which were categorized as either inside or outside of tau envelopes (Fig. 3G). Pairwise comparisons were performed to assess the significance of differences in attachment and detachment frequencies inside versus outside of envelopes for each tau construct.

To determine the dissociation rate constant of kinesins on tau-decorated microtubules, dwell time distributions were fit to a single exponential function according to equation (2):

$$P(t) = A(\, e^{-kt}\,) \tag{2}$$

where *P(t)* is the probability of a kinesin detaching at time *t*, *A* is a normalization constant, and *k* is the dissociation rate constant.

Statistical analysis

All data were presented with error bars indicating either SEM, SD, or 95% CI as specified in the figure legends. All *n* and number of replicates were mentioned in the figure legends. Sample variance significance was determined using a two-sample *F*-test for equal variances in MATLAB. The Wilcoxon signed rank test to test the pairwise comparison of tau intensity in different axonal regions was performed in MATLAB. Bootstrapping analysis was performed in MATLAB and used to test for statistical significance and determine confidence intervals.

Data availability

Source data files for all figures and extended data figures, are available with this manuscript.

Acknowledgements

We thank members of the Hendricks lab for helpful discussions and feedback and Dr Gary Brouhard and Dr Kristen J. Verhey for generously providing reagents. This work was supported by NIH.

Author contributions

D. B., C. L. B., and A. G. H. conceptualization; D. B. formal analysis; D. B. investigation; D. B. and A. G. H. methodology; D. B. and A. G. H. project administration; D. B. and A. G. H. software; D. B. validation; D. B. visualization; D. B. and A. G. H. writing–original draft; D. B., C. L. B., and A. G. H. writing–review and editing; C. L. B. and A. G. H. funding acquisition; C. L. B. and A. G. H. resources; A. G. H. supervision.

Competing interests

The authors declare no competing interests.

References

Ahmad FJ, Pienkowski TP, Baas PW. Regional differences in microtubule dynamics in the axon. J Neurosci. 1993 Feb;13(2):856-66. doi: 10.1523/JNEUROSCI.13-02-00856.1993. PMID: 8426241; PMCID: PMC6576629.

Alushin GM, Lander GC, Kellogg EH, Zhang R, Baker D, Nogales E. High-resolution microtubule structures reveal the structural transitions in αβ-tubulin upon GTP hydrolysis. Cell. 2014 May 22;157(5):1117-29. doi: 10.1016/j.cell.2014.03.053. PMID: 24855948; PMCID: PMC4054694.

Andreadis A, Brown WM, Kosik KS. Structure and novel exons of the human tau gene. Biochemistry. 1992 Nov 3;31(43):10626-33. doi: 10.1021/bi00158a027. PMID: 1420178.

Arpağ G, Norris SR, Mousavi SI, Soppina V, Verhey KJ, Hancock WO, Tüzel E. Motor Dynamics Underlying Cargo Transport by Pairs of Kinesin-1 and Kinesin-3 Motors. Biophys J. 2019 Mar 19;116(6):1115-1126. doi: 10.1016/j.bpj.2019.01.036. Epub 2019 Feb 5. PMID: 30824116; PMCID: PMC6428962.

Baas PW, Slaughter T, Brown A, Black MM. Microtubule dynamics in axons and dendrites. J Neurosci Res. 1991 Sep;30(1):134-53. doi: 10.1002/jnr.490300115. PMID: 1795398.

Balabanian L, Lessard DV, Swaminathan K, Yaninska P, Sébastien M, Wang S, Stevens PW, Wiseman PW, Berger CL, Hendricks AG. Tau differentially regulates the transport of early endosomes and lysosomes. Mol Biol Cell. 2022 Nov 1;33(13):ar128. doi: 10.1091/mbc.E22-01-0018. Epub 2022 Sep 21. PMID: 36129768; PMCID: PMC9634973.

Beaudet D, Berger CL, Hendricks AG. The types and numbers of kinesins and dyneins transporting endocytic cargoes modulate their motility and response to tau. J Biol Chem. 2024 Jun;300(6):107323. doi: 10.1016/j.jbc.2024.107323. Epub 2024 Apr 25. PMID: 38677516; PMCID: PMC11130734.

Bentley M, Decker H, Luisi J, Banker G. A novel assay reveals preferential binding between Rabs, kinesins, and specific endosomal subpopulations. J Cell Biol. 2015 Feb 2;208(3):273-81. doi: 10.1083/jcb.201408056. Epub 2015 Jan 26. PMID: 25624392; PMCID: PMC4315250.

Binder LI, Frankfurter A, Rebhun LI. The distribution of tau in the mammalian central nervous system. J Cell Biol. 1985 Oct;101(4):1371-8. doi: 10.1083/jcb.101.4.1371. PMID: 3930508; PMCID: PMC2113928.

Biswas S, Kalil K. The Microtubule-Associated Protein Tau Mediates the Organization of Microtubules and Their Dynamic Exploration of Actin-Rich Lamellipodia and Filopodia of Cortical Growth Cones. J Neurosci. 2018 Jan 10;38(2):291-307. doi: 10.1523/JNEUROSCI.2281-17.2017. Epub 2017 Nov 22. PMID: 29167405; PMCID: PMC5761611.

Black MM, Cochran JM, Kurdyla JT. Solubility properties of neuronal tubulin: evidence for labile and stable microtubules. Brain Res. 1984 Mar 19;295(2):255-63. doi: 10.1016/0006-8993(84)90974-0. PMID: 6713187.

Brady ST, Tytell M, Lasek RJ. Axonal tubulin and axonal microtubules: biochemical evidence for cold stability. J Cell Biol. 1984 Nov;99(5):1716-24. doi: 10.1083/jcb.99.5.1716. PMID: 6490717; PMCID: PMC2113352.

Brown CL, Maier KC, Stauber T, Ginkel LM, Wordeman L, Vernos I, Schroer TA. Kinesin-2 is a motor for late endosomes and lysosomes. Traffic. 2005 Dec;6(12):1114-24. doi: 10.1111/j.1600-0854.2005.00347.x. PMID: 16262723.

Budaitis BG, Badieyan S, Yue Y, Blasius TL, Reinemann DN, Lang MJ, Cianfrocco MA, Verhey KJ. A kinesin-1 variant reveals motor-induced microtubule damage in cells. Curr Biol. 2022 Jun 6;32(11):2416-2429.e6. doi: 10.1016/j.cub.2022.04.020. Epub 2022 May 2. PMID: 35504282; PMCID: PMC9993403.

Cario A, Savastano A, Wood NB, Liu Z, Previs MJ, Hendricks AG, Zweckstetter M, Berger CL. The pathogenic R5L mutation disrupts formation of Tau complexes on the microtubule by altering local N-terminal structure. Proc Natl Acad Sci U S A. 2022 Feb 15;119(7):e2114215119.

Chaudhary AR, Berger F, Berger CL, Hendricks AG. Tau directs intracellular trafficking by regulating the forces exerted by kinesin and dynein teams. Traffic. 2018 Feb;19(2):111-121. doi: 10.1111/tra.12537. Epub 2017 Dec 5. PMID: 29077261; PMCID: PMC5783771.

Chen J, Kanai Y, Cowan NJ, Hirokawa N. Projection domains of MAP2 and tau determine spacings between microtubules in dendrites and axons. Nature. 1992 Dec 17;360(6405):674-7. doi: 10.1038/360674a0. PMID: 1465130.

Cho JH, Johnson GV. Primed phosphorylation of tau at Thr231 by glycogen synthase kinase 3beta (GSK3beta) plays a critical role in regulating tau's ability to bind and stabilize microtubules. J Neurochem. 2004 Jan;88(2):349-58. doi: 10.1111/j.1471-4159.2004.02155.x. PMID: 14690523.

Chung PJ, Choi MC, Miller HP, Feinstein HE, Raviv U, Li Y, Wilson L, Feinstein SC, Safinya CR. Direct force measurements reveal that protein Tau confers short-range attractions and isoform-dependent steric stabilization to microtubules. Proc Natl Acad Sci U S A. 2015 Nov 24;112(47):E6416-25. doi: 10.1073/pnas.1513172112. Epub 2015 Nov 5. PMID: 26542680; PMCID: PMC4664379.

Dixit R, Ross JL, Goldman YE, Holzbaur EL. Differential regulation of dynein and kinesin motor proteins by tau. Science. 2008 Feb 22;319(5866):1086-9. doi: 10.1126/science.1152993. Epub 2008 Jan 17. PMID: 18202255; PMCID: PMC2866193.

Fan X, Okada K, Lin H, Ori-McKenney KM, McKenney RJ. A pathological phosphorylation pattern enhances tau cooperativity on microtubules and facilitates tau filament assembly. bioRxiv 2025.01.29.635117; doi: https://doi.org/10.1101/2025.01.29.635117.

Feng Q, Mickolajczyk KJ, Chen GY, Hancock WO. Motor Reattachment Kinetics Play a Dominant Role in Multimotor-Driven Cargo Transport. Biophys J. 2018 Jan 23;114(2):400-409. doi: 10.1016/j.bpj.2017.11.016. PMID: 29401437; PMCID: PMC5985011.

Fulga TA, Elson-Schwab I, Khurana V, Steinhilb ML, Spires TL, Hyman BT, Feany MB. Abnormal bundling and accumulation of F-actin mediates tau-induced neuronal degeneration in vivo. Nat Cell Biol. 2007 Feb;9(2):139-48. doi: 10.1038/ncb1528. Epub 2006 Dec 24. PMID: 17187063.

Goedert M, Wischik CM, Crowther RA, Walker JE, Klug A. Cloning and sequencing of the cDNA encoding a core protein of the paired helical filament of Alzheimer disease: identification as the microtubule-associated protein tau. Proc Natl Acad Sci U S A. 1988 Jun;85(11):4051-5. doi: 10.1073/pnas.85.11.4051. PMID: 3131773; PMCID: PMC280359.

Goedert M, Spillantini MG, Potier MC, Ulrich J, Crowther RA. Cloning and sequencing of the cDNA encoding an isoform of microtubule-associated protein tau containing four tandem repeats: differential expression of tau protein mRNAs in human brain. EMBO J. 1989a Feb;8(2):393-9. doi: 10.1002/j.1460-2075.1989.tb03390.x. PMID: 2498079; PMCID: PMC400819.

Goedert M, Spillantini MG, Jakes R, Rutherford D, Crowther RA. Multiple isoforms of human microtubule-associated protein tau: sequences and localization in neurofibrillary tangles of Alzheimer's disease. Neuron. 1989b Oct;3(4):519-26. doi: 10.1016/0896-6273(89)90210-9. PMID: 2484340.

Hasegawa M, Smith MJ, Goedert M. Tau proteins with FTDP-17 mutations have a reduced ability to promote microtubule assembly. FEBS Lett. 1998 Oct 23;437(3):207-10.
Hasegawa M, Smith MJ, Goedert M. Tau proteins with FTDP-17 mutations have a reduced ability to promote microtubule assembly. FEBS Lett. 1998 Oct 23;437(3):207-10.

Hinrichs MH, Jalal A, Brenner B, Mandelkow E, Kumar S, Scholz T. Tau protein diffuses along the microtubule lattice. J Biol Chem. 2012 Nov 9;287(46):38559-68. doi: 10.1074/jbc.M112.369785. Epub 2012 Sep 27. PMID: 23019339; PMCID: PMC3493901.

Hoeprich GJ, Thompson AR, McVicker DP, Hancock WO, Berger CL. Kinesin's neck-linker determines its ability to navigate obstacles on the microtubule surface. Biophys J. 2014 Apr 15;106(8):1691-700. doi: 10.1016/j.bpj.2014.02.034. PMID: 24739168; PMCID: PMC4008791.

Hoeprich GJ, Mickolajczyk KJ, Nelson SR, Hancock WO, Berger CL. The axonal transport motor kinesin-2 navigates microtubule obstacles via protofilament switching. Traffic. 2017 May;18(5):304-314. doi: 10.1111/tra.12478. Epub 2017 Apr 5. PMID: 28267259; PMCID: PMC5687255.

Hoover BR, Reed MN, Su J, Penrod RD, Kotilinek LA, Grant MK, Pitstick R, Carlson GA, Lanier LM, Yuan LL, Ashe KH, Liao D. Tau mislocalization to dendritic spines mediates synaptic dysfunction independently of neurodegeneration. Neuron. 2010 Dec 22;68(6):1067-81. doi: 10.1016/j.neuron.2010.11.030. PMID: 21172610; PMCID: PMC3026458.

Iovino M, Patani R, Watts C, Chandran S, Spillantini MG. Human stem cell-derived neurons: a system to study human tau function and dysfunction. PLoS One. 2010 Nov 11;5(11):e13947. doi: 10.1371/journal.pone.0013947. PMID: 21085657; PMCID: PMC2978712.

Iovino M, Agathou S, González-Rueda A, Del Castillo Velasco-Herrera M, Borroni B, Alberici A, Lynch T, O'Dowd S, Geti I, Gaffney D, Vallier L, Paulsen O, Káradóttir RT, Spillantini MG. Early maturation and distinct tau pathology in induced pluripotent stem cell-derived neurons from patients with MAPT mutations. Brain. 2015 Nov;138(Pt 11):3345-59. doi: 10.1093/brain/awv222. Epub 2015 Jul 27. PMID: 26220942; PMCID: PMC4620511.

Jordens I, Fernandez-Borja M, Marsman M, Dusseljee S, Janssen L, Calafat J, Janssen H, Wubbolts R, Neefjes J. The Rab7 effector protein RILP controls lysosomal transport by inducing the recruitment of dynein-dynactin motors. Curr Biol. 2001 Oct 30;11(21):1680-5. doi: 10.1016/s0960-9822(01)00531-0. PMID: 11696325.

Kanaan NM, Grabinski T. Neuronal and Glial Distribution of Tau Protein in the Adult Rat and Monkey. Front Mol Neurosci. 2021 Apr 27;14:607303. doi: 10.3389/fnmol.2021.607303. PMID: 33986642; PMCID: PMC8112591.

Kanaan NM, Morfini G, Pigino G, LaPointe NE, Andreadis A, Song Y, Leitman E, Binder LI, Brady ST. Phosphorylation in the amino terminus of tau prevents inhibition of anterograde axonal transport. Neurobiol Aging. 2012 Apr;33(4):826.e15-30. doi:

10.1016/j.neurobiolaging.2011.06.006. Epub 2011 Jul 27. PMID: 21794954; PMCID: PMC3272324.

Kanai Y, Chen J, Hirokawa N. Microtubule bundling by tau proteins in vivo: analysis of functional domains. EMBO J. 1992 Nov;11(11):3953-61. doi: 10.1002/j.1460-2075.1992.tb05489.x. PMID: 1396588; PMCID: PMC556906.

Kellogg EH, Hejab NMA, Poepsel S, Downing KH, DiMaio F, Nogales E. Near-atomic model of microtubule-tau interactions. Science. 2018 Jun 15;360(6394):1242-1246. doi: 10.1126/science.aat1780. Epub 2018 May 10. PMID: 29748322; PMCID: PMC6225777.

Li Y, Black MM. Microtubule assembly and turnover in growing axons. J Neurosci. 1996 Jan 15;16(2):531-44. doi: 10.1523/JNEUROSCI.16-02-00531.1996. PMID: 8551337; PMCID: PMC6578637.

Lim SS, Sammak PJ, Borisy GG. Progressive and spatially differentiated stability of microtubules in developing neuronal cells. J Cell Biol. 1989 Jul;109(1):253-63. doi: 10.1083/jcb.109.1.253. PMID: 2745551; PMCID: PMC2115470.

Lindwall G, Cole RD. Phosphorylation affects the ability of tau protein to promote microtubule assembly. J Biol Chem. 1984 Apr 25;259(8):5301-5. PMID: 6425287.

Loubéry S, Wilhelm C, Hurbain I, Neveu S, Louvard D, Coudrier E. Different microtubule motors move early and late endocytic compartments. Traffic. 2008 Apr;9(4):492-509. doi: 10.1111/j.1600-0854.2008.00704.x. Epub 2008 Jan 10. PMID: 18194411.

Mandelkow EM, Biernat J, Drewes G, Gustke N, Trinczek B, Mandelkow E. Tau domains, phosphorylation, and interactions with microtubules. Neurobiol Aging. 1995 May-Jun;16(3):355-62; discussion 362-3. doi: 10.1016/0197-4580(95)00025-a. PMID: 7566345.

Mandelkow EM, Stamer K, Vogel R, Thies E, Mandelkow E. Clogging of axons by tau, inhibition of axonal traffic and starvation of synapses. Neurobiol Aging. 2003 Dec;24(8):1079-85.

McVicker DP, Chrin LR, Berger CL. The nucleotide-binding state of microtubules modulates kinesin processivity and the ability of Tau to inhibit kinesin-mediated transport. J Biol Chem. 2011 Dec 16;286(50):42873-80. doi: 10.1074/jbc.M111.292987. Epub 2011 Oct 27. PMID: 22039058; PMCID: PMC3234877.

McVicker DP, Hoeprich GJ, Thompson AR, Berger CL. Tau interconverts between diffusive and stable populations on the microtubule surface in an isoform and lattice specific manner. Cytoskeleton (Hoboken). 2014 Mar;71(3):184-94. doi: 10.1002/cm.21163. Epub 2014 Feb 24. PMID: 24520046; PMCID: PMC4154625.

Monroy BY, Sawyer DL, Ackermann BE, Borden MM, Tan TC, Ori-McKenney KM. Competition between microtubule-associated proteins directs motor transport. Nat Commun. 2018 Apr 16;9(1):1487. doi: 10.1038/s41467-018-03909-2. PMID: 29662074; PMCID: PMC5902456.

Monroy BY, Tan TC, Oclaman JM, Han JS, Simó S, Niwa S, Nowakowski DW, McKenney RJ, Ori-McKenney KM. A Combinatorial MAP Code Dictates Polarized Microtubule Transport. Dev Cell. 2020 Apr 6;53(1):60-72.e4. doi: 10.1016/j.devcel.2020.01.029. Epub 2020 Feb 27. PMID: 32109385; PMCID: PMC7181406.

Nagpal S, Swaminathan K, Beaudet D, Verdier M, Wang S, Berger CL, Berger F, Hendricks AG. Optogenetic control of kinesin-1, -2, -3 and dynein reveals their specific roles in vesicular transport. Cell Rep. 2024 Aug 27;43(8):114649. doi: 10.1016/j.celrep.2024.114649. Epub 2024 Aug 18. PMID: 39159044; PMCID: PMC11416726.

Niewidok B, Igaev M, Sündermann F, Janning D, Bakota L, Brandt R. Presence of a carboxy-terminal pseudorepeat and disease-like pseudohyperphosphorylation critically influence tau's interaction with microtubules in axon-like processes. Mol Biol Cell. 2016 Nov 7;27(22):3537-3549. doi: 10.1091/mbc.E16-06-0402. Epub 2016 Aug 31. PMID: 27582388; PMCID: PMC5221586.

Okabe S, Hirokawa N. Turnover of fluorescently labelled tubulin and actin in the axon. Nature. 1990 Feb 1;343(6257):479-82. doi: 10.1038/343479a0. PMID: 1689016.

Panda D, Samuel JC, Massie M, Feinstein SC, Wilson L. Differential regulation of microtubule dynamics by three- and four-repeat tau: implications for the onset of neurodegenerative disease. Proc Natl Acad Sci U S A. 2003 Aug 5;100(16):9548-53. doi: 10.1073/pnas.1633508100. Epub 2003 Jul 28. PMID: 12886013; PMCID: PMC170955.

Piras A, Collin L, Grüninger F, Graff C, Rönnbäck A. Autophagic and lysosomal defects in human tauopathies: analysis of post-mortem brain from patients with familial Alzheimer disease, corticobasal degeneration and progressive supranuclear palsy. Acta Neuropathol Commun. 2016 Mar 2;4:22.

Pu J, Guardia CM, Keren-Kaplan T, Bonifacino JS. Mechanisms and functions of lysosome positioning. J Cell Sci. 2016 Dec 1;129(23):4329-4339. doi: 10.1242/jcs.196287. Epub 2016 Oct 31. PMID: 27799357; PMCID: PMC5201012.

Rodríguez-Martín T, Pooler AM, Lau DHW, Mórotz GM, De Vos KJ, Gilley J, Coleman MP, Hanger DP. Reduced number of axonal mitochondria and tau hypophosphorylation in mouse P301L tau knockin neurons. Neurobiol Dis. 2016 Jan;85:1-10.

Rosa-Ferreira C, Munro S. Arl8 and SKIP act together to link lysosomes to kinesin-1. Dev Cell. 2011 Dec 13;21(6):1171-8. doi: 10.1016/j.devcel.2011.10.007. PMID: 22172677; PMCID: PMC3240744.

Rosenberg KJ, Ross JL, Feinstein HE, Feinstein SC, Israelachvili J. Complementary dimerization of microtubule-associated tau protein: Implications for microtubule bundling and tau-mediated pathogenesis. Proc Natl Acad Sci U S A. 2008 May 27;105(21):7445-50. doi: 10.1073/pnas.0802036105. Epub 2008 May 21. PMID: 18495933; PMCID: PMC2396711.

Sahenk Z, Brady ST. Axonal tubulin and microtubules: morphologic evidence for stable regions on axonal microtubules. Cell Motil Cytoskeleton. 1987;8(2):155-64. doi: 10.1002/cm.970080207. PMID: 2891447.

Schneider A, Biernat J, von Bergen M, Mandelkow E, Mandelkow EM. Phosphorylation that detaches tau protein from microtubules (Ser262, Ser214) also protects it against aggregation

into Alzheimer paired helical filaments. Biochemistry. 1999 Mar 23;38(12):3549-58. doi: 10.1021/bi981874p. PMID: 10090741.

Siahaan V, Krattenmacher J, Hyman AA, Diez S, Hernández-Vega A, Lansky Z, Braun M. Kinetically distinct phases of tau on microtubules regulate kinesin motors and severing enzymes. Nat Cell Biol. 2019 Sep;21(9):1086-1092. doi: 10.1038/s41556-019-0374-6. Epub 2019 Sep 2. PMID: 31481789.

Siahaan V, Tan R, Humhalova T, Libusova L, Lacey SE, Tan T, Dacy M, Ori-McKenney KM, McKenney RJ, Braun M, Lansky Z. Microtubule lattice spacing governs cohesive envelope formation of tau family proteins. Nat Chem Biol. 2022 Nov;18(11):1224-1235. doi: 10.1038/s41589-022-01096-2. Epub 2022 Aug 22. PMID: 35996000; PMCID: PMC9613621.

Siahaan V, Weissova R, Lanska E, Karhanova A, Dostal V, Henriot V, Janke C, Libusova L, Braun M, Balastik M, Lansky Z. Tau phosphorylation impedes functionality of protective tau envelopes. bioRxiv 2024.03.25.586522; doi: https://doi.org/10.1101/2024.03.25.586522.

Song Y, Kirkpatrick LL, Schilling AB, Helseth DL, Chabot N, Keillor JW, Johnson GV, Brady ST. Transglutaminase and polyamination of tubulin: posttranslational modification for stabilizing axonal microtubules. Neuron. 2013 Apr 10;78(1):109-23. doi: 10.1016/j.neuron.2013.01.036. PMID: 23583110; PMCID: PMC3627183.

Sposito T, Preza E, Mahoney CJ, Setó-Salvia N, Ryan NS, Morris HR, Arber C, Devine MJ, Houlden H, Warner TT, Bushell TJ, Zagnoni M, Kunath T, Livesey FJ, Fox NC, Rossor MN, Hardy J, Wray S. Developmental regulation of tau splicing is disrupted in stem cell-derived neurons from frontotemporal dementia patients with the 10 + 16 splice-site mutation in MAPT. Hum Mol Genet. 2015 Sep 15;24(18):5260-9. doi: 10.1093/hmg/ddv246. Epub 2015 Jul 1. PMID: 26136155; PMCID: PMC4550814.

Stamer K, Vogel R, Thies E, Mandelkow E, Mandelkow EM. Tau blocks traffic of organelles, neurofilaments, and APP vesicles in neurons and enhances oxidative stress. J Cell Biol. 2002 Mar 18;156(6):1051-63. doi: 10.1083/jcb.200108057. Epub 2002 Mar 18. PMID: 11901170; PMCID: PMC2173473.

Steinhilb ML, Dias-Santagata D, Mulkearns EE, Shulman JM, Biernat J, Mandelkow EM, Feany MB. S/P and T/P phosphorylation is critical for tau neurotoxicity in Drosophila. J Neurosci Res. 2007 May 1;85(6):1271-8. doi: 10.1002/jnr.21232. PMID: 17335084.

Stern JL, Lessard DV, Hoeprich GJ, Morfini GA, Berger CL. Phosphoregulation of Tau modulates inhibition of kinesin-1 motility. Mol Biol Cell. 2017 Apr 15;28(8):1079-1087. doi: 10.1091/mbc.E16-10-0728. Epub 2017 Mar 1. PMID: 28251926; PMCID: PMC5391184.

Stokin GB, Lillo C, Falzone TL, Brusch RG, Rockenstein E, Mount SL, Raman R, Davies P, Masliah E, Williams DS, Goldstein LS. Axonopathy and transport deficits early in the pathogenesis of Alzheimer's disease. Science. 2005 Feb 25;307(5713):1282-8.

Tan R, Lam AJ, Tan T, Han J, Nowakowski DW, Vershinin M, Simó S, Ori-McKenney KM, McKenney RJ. Microtubules gate tau condensation to spatially regulate microtubule functions. Nat Cell Biol. 2019 Sep;21(9):1078-1085. doi: 10.1038/s41556-019-0375-5. Epub 2019 Sep 2. PMID: 31481790; PMCID: PMC6748660.

Trinczek B, Biernat J, Baumann K, Mandelkow EM, Mandelkow E. Domains of tau protein, differential phosphorylation, and dynamic instability of microtubules. Mol Biol Cell. 1995 Dec;6(12):1887-902. doi: 10.1091/mbc.6.12.1887. PMID: 8590813; PMCID: PMC366657.

Vershinin M, Carter BC, Razafsky DS, King SJ, Gross SP. Multiple-motor based transport and its regulation by Tau. Proc Natl Acad Sci U S A. 2007 Jan 2;104(1):87-92. doi: 10.1073/pnas.0607919104. Epub 2006 Dec 26. PMID: 17190808; PMCID: PMC1765483.

Vershinin M, Xu J, Razafsky DS, King SJ, Gross SP. Tuning microtubule-based transport through filamentous MAPs: the problem of dynein. Traffic. 2008 Jun;9(6):882-92. doi: 10.1111/j.1600-0854.2008.00741.x. Epub 2008 Mar 28. PMID: 18373727; PMCID: PMC2958055.

Weingarten MD, Lockwood AH, Hwo SY, Kirschner MW. A protein factor essential for microtubule assembly. Proc Natl Acad Sci U S A. 1975 May;72(5):1858-62. doi: 10.1073/pnas.72.5.1858. PMID: 1057175; PMCID: PMC432646.